Cite this article
Heins E, Bienen B, Randolph MF and Grabe J (2020)
Effect of installation method on static and dynamic load test response for piles in sand.
International Journal of Physical Modelling in Geotechnics **20(1)**: 1–23,
https://doi.org/10.1680/jphmg.18.00028

Research Article
Paper 1800028
Received 09/05/2018;
Accepted 07/10/2018;
Published online 06/11/2018

Keywords: dynamics/granular materials/ foundations

International Journal of Physical Modelling in Geotechnics

ice Publishing

Effect of installation method on static and dynamic load test response for piles in sand

Evelyn Heins
Research Assistant, Institute of Geotechnical Engineering and Construction Management, Hamburg University of Technology, Hamburg, Germany (corresponding author: evelyn.heins@tuhh.de)
(Orcid:0000-0001-8920-3864)

Britta Bienen
Associate Professor, Centre for Offshore Foundation Systems, the University of Western Australia, Crawley, Perth, WA, Australia

Mark F. Randolph
Professor, Centre for Offshore Foundation Systems, the University of Western Australia, Crawley, Perth, WA, Australia

Juergen Grabe
Professor, Institute of Geotechnical Engineering and Construction Management, Hamburg University of Technology, Hamburg, Germany

Static load tests (SLTs) are rarely performed on offshore piles, instead relying on dynamic load tests (DLTs). Evaluation techniques for DLTs were developed originally for solid piles, and caution is needed in applying the techniques directly to open-ended piles, particularly for the large-diameter monopiles used for offshore wind turbines. Centrifuge tests are reported here, investigating the influence of pile installation method and sand relative density for pairs of DLTs and SLTs. The piles were successfully driven to penetration of 3–4·6 diameters, which was much deeper than proved possible to jack the piles. Due to limited hammer energy, loads mobilised during the DLTs were less than 25% of the corresponding SLT values. The soil resistance mobilised at limited displacements was lowest for wished-in-place piles, and also for DLTs conducted on shallowly embedded jacked piles. For driven piles, the DLT and SLT results were relatively consistent, with surprisingly similar values for piles driven into loose and dense sand despite significant differences in cone resistance. Given the potential for low mobilisation of soil resistance in DLTs, care is needed when using DLTs for evaluating the static axial pile capacity of open-ended piles of low length-to-diameter ratio.

Notation

A	area (m^2)
a	acceleration (m/s^2)
c_{PVC}	wave velocity within a polyvinyl chloride strip (m/s)
c_v	wave speed (m/s)
D	diameter (m)
D_a	outer diameter (m)
D_{cone}	diameter of cone used during cone penetration test (m)
d_50	mean particle size (mm)
E	bulk modulus (kPa)
EA	axial stiffness (kN)
F	force (kN)
F_1	force at time t_1 during a dynamic load test (kN)
F_2	force at time t_2 during a dynamic load test (kN)
$\boldsymbol{g}$	gravitational acceleration (m/s^2)
I_D	relative density
j_c	damping factor
L	length (m)
L_e	embedment depth (m)
n	scaling factor for centrifuge tests
q_c	cone resistance during cone penetration test (kPa)
SR	mobilised soil resistance (kN)
t	time (s)
t_1	time when wave passes sensors for the first time during a dynamic load test (s)
t_2	time when wave passes sensors for the second time during a dynamic load test (s)
U	index of uniformity
v	velocity (m/s)
v_1	velocity at time t_1 during a dynamic load test (m/s)
v_2	velocity at time t_2 during a dynamic load test (m/s)
v_{CPT}	velocity during a cone penetration test (m/s)
Z	impedance
z	distance below ground surface (m)
$\gamma_{d,min}$	minimum dry density (kN/m^3)
$\gamma_{d,max}$	maximum dry density (kN/m^3)
Δt	time difference (s)
Δz	penetrated depth below ground surface (m)
ε	strain
ρ	density (t/m^3)
σ'_v	effective stresses (kPa)
ϕ_c	critical state friction angle (degree)

1. Motivation

Much of offshore energy infrastructure is founded on (large-diameter) open-ended piles installed to relatively low length-to-diameter (L/D) ratios. Common design guidelines (e.g. Eurocode 7-1 (DIN, 2014) and the design standard of the German Federal Maritime and Hydrographic Agency (BSH) (BSH, 2015)) require verification of the static pile bearing

capacity under compression load after pile installation on site. Consequently, pile contracts include the execution of pile load tests.

Ideally, the static axial bearing capacity should be obtained from static load tests (SLTs). The static bearing capacity of a pile is a function of many factors, including the relative density of the soil, the pile geometry and penetration depth, the installation method and, for rapid loading, the soil–fluid interaction. Substantial knowledge of the static bearing capacity of open-ended piles is available from extensive research for example by Paikowsky and Whitman (1990), Hartung (1994), de Nicola and Randolph (1997), Lehane and Gavin (2001), Paik *et al*. (2003), Deeks *et al*. (2005), Schneider *et al*. (2005), Jardine *et al*. (2005), Clausen *et al*. (2005) and Henke and Grabe (2013). However, SLTs are generally not performed offshore due to practical and economic reasons. A well-established alternative to SLTs are dynamic load tests (DLTs), from which the static pile bearing capacity may be deduced. Experience in evaluating the static capacity from dynamic pile head data from DLTs has largely been developed on closed-ended piles. However, open-ended piles have a distinctly different behaviour compared with solid (or close-ended) piles, resulting from the more complex pile–soil interaction on the inside of the pile (Bruno and Randolph, 1999; Paikowsky and Chernauskaus, 2008; Randolph, 2003). Under static loading, the pile will respond in a partially or fully plugged manner (i.e. with limited slip between the internal soil and the pile), while during a DLT, the pile advances by shearing on both internal and external shaft surfaces and mobilisation of resistance at the annular pile tip. The internal shaft friction may differ significantly from the external shaft friction due to different radial stress states of the soil inside and outside the pile, which may also be affected by arching mechanisms within the soil plug. Investigations by Paikowsky and Chernauskaus (2008) revealed that the wave propagation inside the pile–soil system involving an open-ended pile cannot strictly be captured by the one-dimensional wave theory that is applied to close-ended piles. This is supported by numerical studies by Grabe and Heins (2016). Results of the numerical simulations show an influence of different pile–soil interaction properties resulting from different states of plugging as well as of varying drainage conditions in the soil. Improved understanding of dynamic pile–soil interaction within the soil plug is needed in order to derive realistic static bearing capacities for open-ended piles from DLTs.

The main objective of this study was to obtain data from physical model tests, comparing results from static and DLTs, in order to validate numerical findings and to improve understanding of the behaviour of open-ended piles during DLTs. Model tests allow detailed investigation of SLTs and DLTs under well-defined soil conditions. For relevance to prototype piles, the experiments discussed in this paper were performed at 100$\boldsymbol{g}$ on a geotechnical centrifuge, modelling 5 m diameter piles embedded between 1·8 and 4·6 diameter, primarily in relatively loose sand. The tests explored the effect of pile installation method, embedment depth, state of soil plugging, sand relative density and soil saturation conditions on the pile response.

2. Dynamic load test

During a DLT, a dynamic impact is applied to the pile head by means of a hammer blow. This dynamic impact is usually performed by executing one hammer blow, causing a stress wave to propagate through the pile (Figure 1(a)). Due to the large difference in density between pile and soil, the resulting wave is reflected at the pile tip. Figure 1(b) shows pile head signals resulting from wave propagation of open-ended piles with different states of plugging. These curves are based on the following understanding and are taken from the test results. The nature of the returning wave is affected by the resistance mobilised at the pile tip. Thus, the signal characteristics of a fully plugged open-ended pile feature a compression wave propagating downward through the pile, which is reflected at the (assumed high resistance) pile tip as a compression wave. This results in an increase in the compression force being registered at the pile head as the stress-wave returns. The fully plugged open-ended pile is assumed to have a high tip resistance, and therefore shows a compression wave at time t_2 within the schematic example of Figure 1(b). By contrast, an unplugged open-ended pile, with low soil resistance mobilised at the pile tip, would lead to a tensile reflected wave, and hence a reduction in the compression force (and potentially a tensile force as shown at t_2 for pile test T2 in Figure 1(b)) being registered near the pile head as the stress-wave returns. The pile head signal for a partially plugged pile may be assumed to lie between these two, as shown in Figure 1(b) (test T13).

It is assumed that the wave propagation may be approximated as one dimensional within the pile, given the much higher stiffness (and wave propagation speed) of the pile compared with the soil. During a DLT, the wave propagation through the pile is measured over time in terms of strain $\varepsilon(t)$ and acceleration $a(t)$ at the pile head. The process of wave propagation down the pile, followed by reflection at the tip and propagation back up as the pile head signal is shown in Figure 1(a). The dynamic pile head signals may be interpreted in order to derive the static bearing capacity under compression load of the tested pile (EA-Pfähle, 2012; Randolph and Deeks, 1992; Rausche *et al*., 2010).

Evaluation of pile head signals from DLTs on close-ended piles is well established (Stahlmann *et al*., 2004). The measured

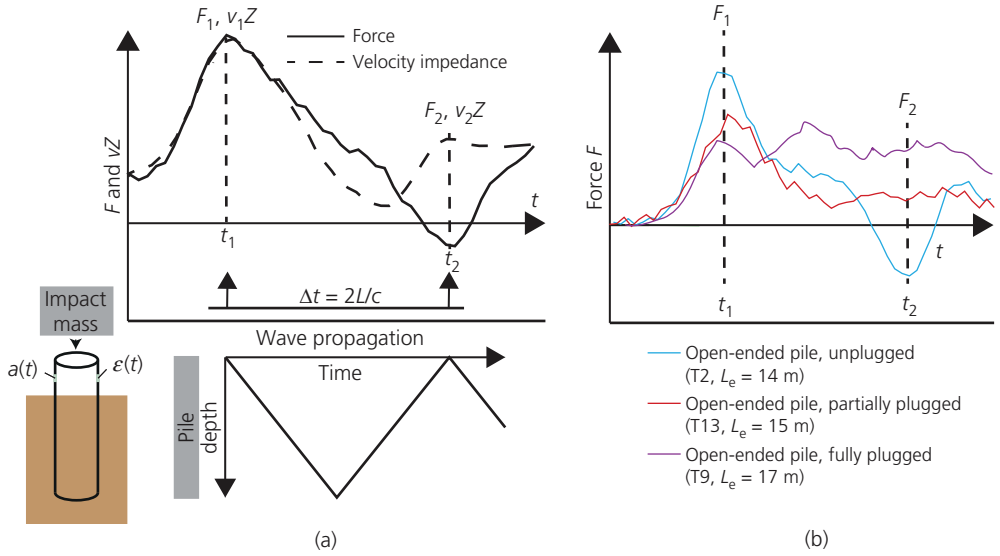

Figure 1. Schematic example pile head signals. (a) Taken from test T1, (b) expected pile head signal

acceleration $a(t)$ and strain $\varepsilon(t)$ are transferred to force and velocity

1. $$F(t) = \varepsilon(t)\mathrm{EA}$$

2. $$v(t) = \int_0^t a(t)\mathrm{d}t$$

Velocity is converted into a force by multiplication by the impedance of the pile Z, where Z is the ratio of the cross-sectional stiffness (EA) of the pile material to the wave propagation speed c. This force is the so-called impedance force vZ.

The wave propagation through a solid pile can be described based on one-dimensional wave theory (Paikowsky and Chernauskaus, 2008). Therefore, the pile–soil-interaction problem is reduced to wave propagation within a one dimensional, embedded rod. By simplifying the problem differential equations can be derived. This approach is used in different evaluation techniques. For solid piles, EA-Pfähle (2012) differentiates between 'advanced' and 'direct' methods. Within the 'direct' methods, simple analytical equations are established. Using pile head signals, the soil resistance mobilised during the blow is derived from these relationships directly. Examples for the 'direct' methods as explained in EA-Pfähle (2012) are the TNO and CASE methods as well as the method according to Kolymbas (1991).

'Advanced' methods transfer the system to a numerical model. These methods are described in detail for example in EA-Pfähle (2012), Rausche *et al.* (2010), Stahlmann *et al.* (2004), Randolph (2003) and Randolph and Deeks (1992). The pile–soil system is modelled with springs, point masses, dampers and sliders for the soil and linear-elastic, one-dimensional elements for the pile. The required parameters to define the behaviour of the rheological elements used to describe the soil such as spring stiffness and damper coefficient are unknown variables in the numerical system. The spring–damper elements along the pile shaft define skin friction and characteristic curves for the spring–damper elements define the tip resistance.

To obtain the pile bearing capacity, an inverse calculation is carried out when using the 'advanced' methods. Different approaches exist for this. One approach is to define the force F measured at pile head as the input to the numerical model. The impedance force vZ is calculated with the described model. Another approach is to use the downward travelling component $(F + vZ)/2$ as the input and to calculate the upward travelling component $(F - vZ)/2$. A signal matching between measured and calculated signals is conducted, varying the unknown parameters of the system until a best fit is achieved. The parameter values obtained may then be used to simulate a SLT. The solution for the signal matching is not unique and the results are user dependent. Therefore, prior knowledge and sufficient experience is required to derive the pile bearing capacity applying 'advanced' methods. Examples for these methods are CAPWAP (developed by GRL, Goble Rausche Likins and Associates, Inc.) and ALLWAVE (developed by Allnamics).

The stress-wave analysis approach described above has been developed for close-ended piles, and they are generally applied to open-ended piles by simply lumping together internal and external frictional response on the outside of the pile. Although more sophisticated models, with the soil column within the pile treated independently (Heerema and de Jong, 1979), they are rarely used in practice. As such, there is limited understanding of the interaction of open-ended piles with the soil during driving, or the interpretation of DLTs on open-ended piles. This paper addresses this gap on the basis of pairs of DLTs and SLTs of open-ended piles tested in the centrifuge.

3. Centrifuge modelling

The *ng*-physical model tests were performed in a fixed beam geotechnical centrifuge of type 661 with a platform radius of 1·8 m at the Centre for Offshore Foundation Systems at the University of Western Australia.

3.1 Soil sample and pore fluid

A total of seven sand samples were prepared to a target soil sample height of 0·31 m in strongboxes of 0·39 m internal width, 0·65 m length and 0·425 m height. While no specific sand relative density was targeted, the actuator capacity was known to be the limiting factor. Hence, samples as loose as practical were prepared by carefully pouring the sand into the strongbox manually from a scoop with minimum falling height. A significantly higher relative density was achieved by dry pluviation of the sand. The programme comprised of pile tests conducted in the following samples

- dry, loose sand (three samples)
- cellulose ether saturated, loose sand (two samples)
- water saturated, loose sand (one sample)
- dry, dense sand (one sample), which was subsequently saturated with water.

Generally, two piles were installed in each sample, with DLTs and SLTs conducted on each.

Table 1 provides an overview of all sand samples and pile tests.

The mechanical properties of the very fine silica sand used for testing are listed in Table 2.

Diffusion processes take place in centrifuge tests n^2 faster than at prototype scale, while the loading rate scales by a factor of n. In order to achieve prototype conditions very high loading frequencies are necessary during testing with a water-saturated sample. Alternatively, in order to maintain practically achievable loading frequencies, the viscosity of the pore fluid can be raised by a factor of n. This approach is successfully established for centrifuge tests of earthquake engineering (Abdoun *et al.*, 2003; Lee *et al.*, 2014; Sharp *et al.*, 2003), offshore foundations (Andersen *et al.*, 1994; Bienen *et al.*, 2018) and has been used here. Hence, a mixture of water and cellulose ether creating a 100 cst viscosity fluid at a temperature of 20°C was used in some of the centrifuge tests performed, maintaining the characteristics, behaviour and density of water apart from the increased viscosity.

For the purpose of evaluating the influence of significantly different hydraulic conductivities, another two samples, one loose and one dense sample, were saturated with water.

Within each soil sample four cone penetration tests (CPTs) with a penetrometer of diameter $D_{cone} = 10$ mm were performed (at a minimum distance of 7·5 D_{cone} from the side of the strongbox) to verify the homogeneity and repeatability of the samples. The cone was penetrated vertically into the soil sample with a constant velocity of $v_{cpt} = 0{\cdot}5$ mm/s, which was evaluated as the limiting condition resulting in drained behaviour in all samples, according to the criterion by Finnie and Randolph (1994)

$$\frac{v_{cpt} D_{cone}}{c_v} < 0{\cdot}01 \quad (3)$$

where v_{cpt} is the cone penetration velocity, D_{cone} the cone diameter and c_v the coefficient of consolidation, which was assumed as 520 mm^2/s (16 000 m^2/year) for a loose, cellulose ether saturated sample.

Figure 2 shows the results of all 28 CPTs conducted. The measured cone resistance has been normalised by the effective vertical stress σ'_v and plotted against depth below ground surface (z) normalised by outer pile diameter (D_a, which is 5 times the cone diameter, D_{cone}). The effective vertical stress σ'_v is calculated using a density of $\rho' = 1{\cdot}5$ t/m^3 for dry and $\rho' = 1{\cdot}0$ t/m^3 for saturated soil samples. The different CPT data are differentiated by boxes (see Table 1).

The cone tip resistances for the loose samples all lie within a relatively narrow band and suggest an average relative density of $I_D = 0{\cdot}34$ for saturated and dry samples. For the soil samples containing wished-in-place piles (boxes 2 and 6) a slightly higher relative density of $I_D = 0{\cdot}39$ was achieved compared with the other loose samples. This reveals the difficulty of creating soil samples with the pile already in place. The CPT results for the dense samples suggest average relative densities of $I_D = 0{\cdot}70$. To characterise the soil samples for the different performed test scenarios, Table 1 provides measured CPT data q_c at the depth of the performed SLT and an averaged value of q_c, which averages all measured CPT data of the considered soil sample up to the depth of the performed SLT.

Table 1. Overview of the performed test as well as test labels

Test	Soil sample	Pile installation method	Depth of DLT	Depth of SLT	q_c at depth of SLT: MPa	q_c averaged over depth and sample: MPa
T1	Loose, dry (box 1)	Jacked	$2D_a$, $2{\cdot}2D_a$	$2D_a$	4·4	1·9
T2	Loose, dry (box 1)	Impact driven	$2{\cdot}8D_a$, $4D_a$	$4D_a$	7·4	4·2
T3	Loose, dry (box 2)	Wished-in-place	$4{\cdot}6D_a$	$4{\cdot}6D_a$	10·8	6·1
T4	Loose, dry (box 2)	Impact driven	$2{\cdot}8D_a$, $4D_a$	$4D_a$	9·5	5·5
T5	Loose, dry (box 3)	Impact driven	$4{\cdot}4D_a$	$4{\cdot}4D_a$	8·8	3·8
T6	Loose, water saturated (box 4)	Jacked	—	$1{\cdot}8D_a$	3·0	1·0
T7	Loose, water saturated (box 4)	Impact driven	$3D_a$	$3D_a$	4·1	1·3
T8	Loose, cellulose ether saturated (box 5)	Jacked	$2{\cdot}4D_a$, $2{\cdot}6D_a$	$2{\cdot}4D_a$	4·2	1·2
T9	Loose, cellulose ether saturated (box 5)	Impact driven	$3D_a$, $3{\cdot}4D_a$	$3{\cdot}4D_a$	5·5	1·6
T10	Loose, cellulose ether saturated (box 6)	Wished-in-place	$4{\cdot}6D_a$	$4{\cdot}6D_a$	7·3	4·4
T11	Loose, cellulose ether saturated (box 6)	Impact driven	$2{\cdot}2D_a$	$2{\cdot}2D_a$	4·8	0·9
T12	Dense, dry (box 7)	Impact driven	$3{\cdot}1D_a$	$3{\cdot}1D_a$	33·0	15·3
T13	Dense, water saturated (box 7)	Impact driven	$3D_a$	$3D_a$	26·6	11·8

Table 2. Mechanical properties of very fine silica sand

Parameter	Value	Description: unit
d_{50}	0·19	Mean particle size: mm
U	1·9	Index of uniformity
ϕ_c	30	Critical state friction angle: degree
$\gamma_{d,min}$	14·9	Minimum dry density: kN/m^3
$\gamma_{d,max}$	18·0	Maximum dry density: kN/m^3

Taken from Pucker *et al.* (2013)

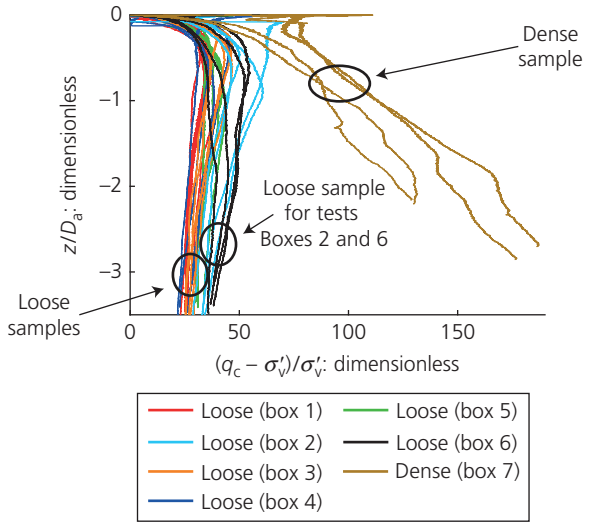

Figure 2. CPT results

3.2 Model pile and instrumentation

The prototype monopile studied for these centrifuge tests is a large-diameter tubular steel pile with an outer diameter of $D_a = 5{\cdot}0$ m. Geometric similarity between prototype monopile and model pile is established by linearly scaling the pile diameter to $D_a = 50$ mm. The target embedment ratio D_a/L_e was 5, which is typical for offshore monopiles. The dynamic response, important for DLT, is characterised by wave propagation through the pile, which is influenced by the axial stiffness EA. Similitude to the prototype is hence upheld by selecting a wall thickness of 1·6 mm for the aluminium model pile. It is acknowledged that this represents a wall thickness that is slightly larger than typical in the prototype, and that this may influence the ratio between tip resistance and shaft friction. However, the tendency for pile plugging, likely a key influence in the pile response, is not expected to be affected.

The pile was instrumented with strain gauges and a MEMS 3501A1260KG accelerometer with a measurement range of 60 000$\boldsymbol{g}$ in order to capture the response during installation, DLT and SLT. According to EA-Pfähle (2012), the distance between the load application and the measurement devices should be larger than 1·5 D_a in order to measure a plain wave propagation. Hence, the sensors were located at model scale 80 mm (1·6 D_a) below load application as shown in Figure 3.

Measurements of acceleration at small scale are difficult (Bruno and Randolph, 1999) and can be influenced by oscillations and resonance effects. This was indeed found to be the case. Further, as the measured accelerations remained well below 60 000$\boldsymbol{g}$, the signal was deemed unreliable and the MEMS data were eventually discarded.

A Hopkinson bar as employed by Bruno and Randolph (1999) was used as a secondary measurement device from which to assess the local pile velocity. The Hopkinson bar as illustrated in Figure 3(c) consisted of a 220 mm long, 3 mm wide and 1·6 mm thick poly vinyl chloride (PVC) strip to which two adjacent strain gauges are attached. The stress wave travelling through the pile causes wave propagation along the PVC strip.

The return time of the wave within the Hopkinson bar is longer than the return time of the wave in the pile. Therefore, the downward-travelling stress wave in the pile, and its modification, by the return wave is measured by the Hopkinson bar without influence from the return wave in the Hopkinson bar. The strain measured by the Hopkinson bar can be converted to pile velocity v by multiplication with the wave speed in the Hopkinson bar c_{pvc}

$$v = \varepsilon c_{pvc} \quad (4)$$

For these tests a wave speed in the Hopkinson bar of $c_{pvc} = 1453{\cdot}5$ m/s is relevant.

3.3 Testing arrangement

The pile was positioned $3D_a$ from the end of the strongbox along the centreline (cf. Figure 4), which allowed two tests to be performed per soil sample. A spacing of $1{\cdot}2\ D_a$ below the pile tip remained at the target embedment length of $L_e = 5\ D_a$. Due to the restricted size of the soil sample wave reflection during pile installation from the strongbox walls could not be prevented. However, the spacing between pile and model boundaries was sufficiently large to exclude effects from wave reflection during time span of the DLTs.

The pile as shown in Figure 4 was connected to the anvil of a miniature pile driving hammer by way of an axial load cell. The pneumatic miniature pile driving hammer is described in De Nicola and Randolph (1994). Here, the drop weight of the pile driving hammer was 50 g at model scale, corresponding to a 50 t prototype hammer, which was used in combination with a targeted constant drop height of 17 mm (model scale). (As noted later, however, this drop height was not achieved, due to insufficient air supply to lift the hammer ram.) The pile driving hammer was mounted on the carriage of a dual-axis servo-controlled actuator. The vertical pile displacement was measured by a displacement transducer (Figure 4), with a feedback loop allowing the actuator (and hence the pile driving hammer) to follow the penetrating pile. The horizontal position was maintained by disabling the horizontal actuator movement.

3.4 Testing procedure

The response of the pile during a DLT to varying drainage conditions of the soil, different initial densities of the soil, different installation methods and various installation depths is investigated. After accelerating the centrifuge to 100***g***, set to act at a distance of $1/3L_e$ below the soil surface, pile installation was performed, followed by a pair of DLT and SLT. The following pile installation methods were considered

- Wished-in-place, a scenario with no influences of the installation process. The entire testing apparatus was in place when the sand sample was created, with the pile held at the target depth for the pair of DLT and SLT to be performed.
- Jacking – a static pile installation method. Pile jacking was achieved by penetrating the pile into the soil with the

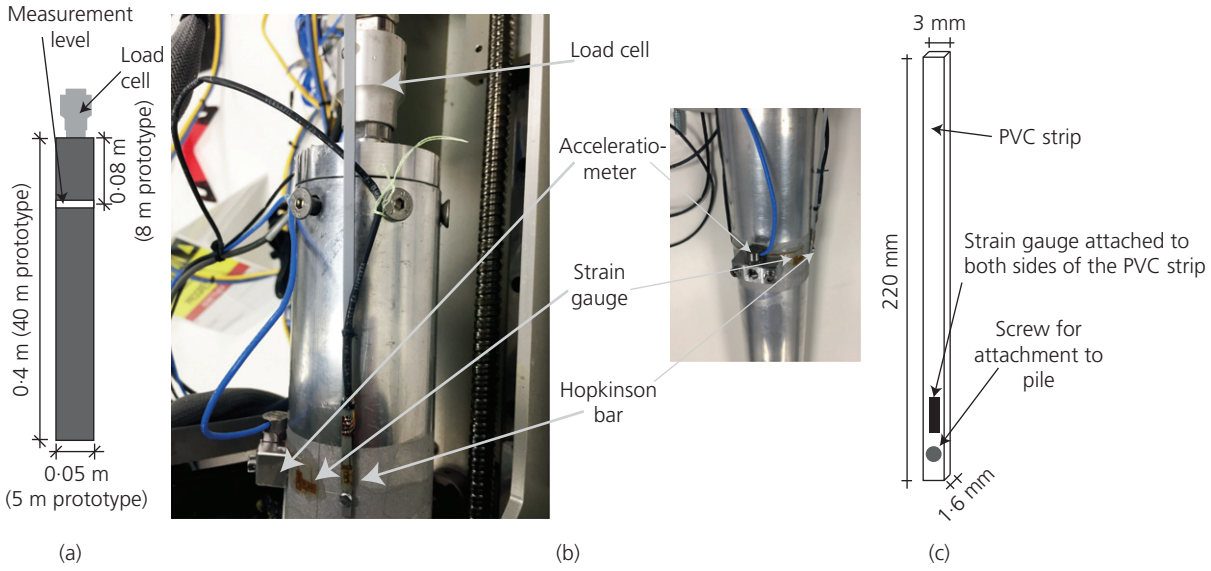

Figure 3. Instrumentation of the model pile with accelerometer, strain gauge and Hopkinson bar at pile head: (a) schematic pile instrumentation, (b) photograph of pile instrumentation and (c) sketch of Hopkinson bar

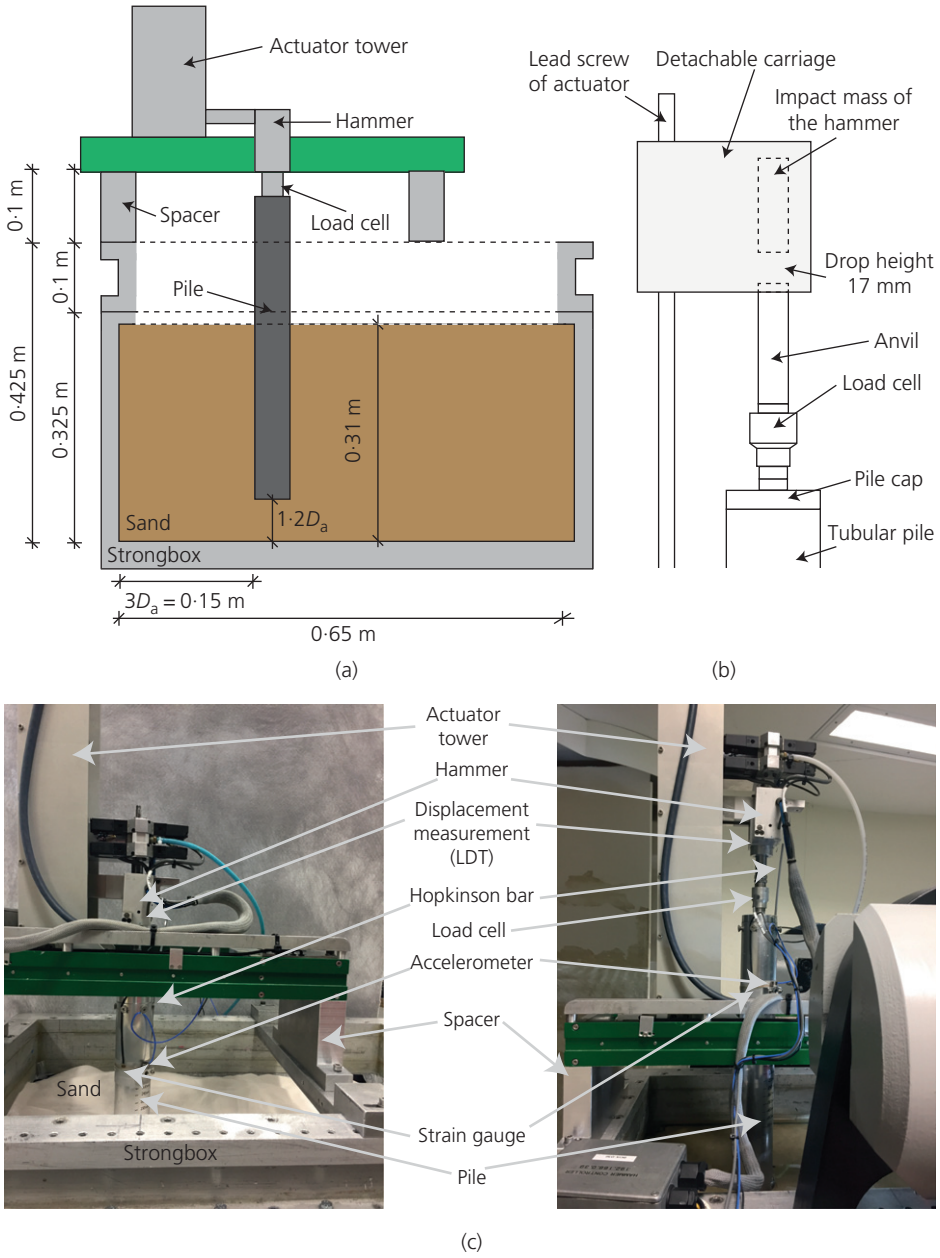

Figure 4. (a) Schematic drawing of testing arrangement, (b) schematic drawing of hammer–pile connection and (c) photograph of testing arrangement

actuator (through the pile driving hammer) at a constant vertical velocity of $v = 0{\cdot}1$ mm/s, which ensured drained conditions (cf. Equation 3). The jacking process was stopped when the resistance approached 5 kN, ensuring sufficient remaining actuator capacity for a SLT.

- Impact pile driving, which is the most common dynamic method of offshore pile installation. A frequency of 5 Hz (0·05 Hz at prototype scale) was maintained during continuous operation of the pile driving hammer. The installation process was terminated when the pile achieved no further penetration with the set driving characteristics.

A wait time of at least 120 s (model scale) following pile installation was used in every test to prevent influences from waves propagating through the apparatus and excess pore-water pressures in the soil caused by the installation procedure.

Then, a DLT, consisting of a single hammer blow, was performed. This resulted in a stress wave travelling through the pile, with corresponding measurements of strain and velocity, which were acquired at a data sampling frequency of 200 kHz. After another wait time of at least 600 s, a SLT was conducted to enable comparison between DLT and SLT results. During the SLT, the pile was jacked at a constant velocity of $v = 0{\cdot}1$ mm/s ensuring drained conditions. The SLT was terminated at a displacement of $0{\cdot}1D_a$ or when the actuator capacity was reached.

Within each soil sample (box), one impact-driven pile installation was performed to enable a cross-comparison of the results between the boxes. A total of 13 tests were performed, with Table 1 providing an overview of the sample number, sand relative density and saturation, the pile installation method and the penetration depth at which the DLT and SLT were performed. Figure 5 provides a graphical overview.

The target prototype installation depth of $L_e = 25{\cdot}0$ m could not be reached. Therefore, the embedment depth for the wished-in-place piles was adjusted to $L_e = 23{\cdot}0$ m at prototype scale. All other piles were installed to the greatest depth possible. Additional DLTs were performed at a prototype embedment length of $L_e = 12{\cdot}0$ m for all tests with greater possible pile installation depth to allow a cross-comparison between the results of the DLTs at similar depths. This is relevant for T2, T4 and T9.

4. Results

4.1 Notation

The results of the static and DLTs that followed pile installation are presented in terms of depth below ground surface z, penetrated depth below pile installation depth Δz, outer pile diameter D_a, embedment length of the pile L_e, cone resistance q_c, relative density I_D as well as measured forces during SLT F and during DLT (F, vZ). The forces of the DLT are derived quantities. The measurements of strain on the pile and velocity from the Hopkinson bar are transferred to force F and impedance force vZ as time series. The results shown in this section are in prototype scale. The SLT and DLT measurements for the wished-in-place pile in a loose, dry sample (T3) do not seem reasonable. The bottom support appears not to have functioned properly, possibly allowing the pile to deviate from vertical and resulting in poor quality data. An evaluation of these data sets has not been performed.

4.2 Static load tests

An overview of the available data of all SLT is given in Figure 6, exhibiting the expected increasing trend with additional penetration. The results of static resistance mobilised at displacements of $0{\cdot}05\ D_a$ and at $0{\cdot}1\ D_a$ as well as the initial gradient are summarised in Table 3. (The slight unevenness occurring in all tests at approximately $F = 15$ MN and $F = 25$ MN is caused by seating within the connection between pile and hammer.)

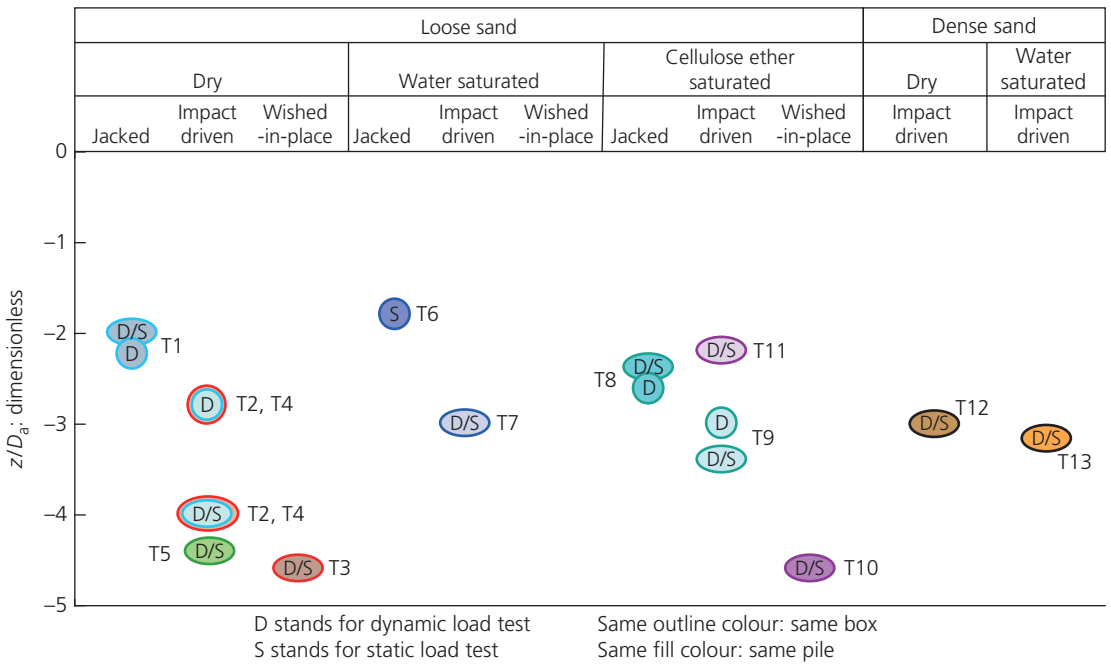

Figure 5. Overview of centrifuge pile tests

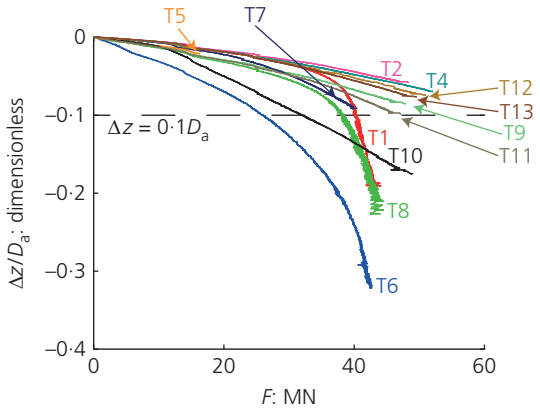

Figure 6. All obtained SLT results

4.2.1 Effect of installation method on SLTs in loose sand – no installation

As three different pile installation methods were employed in the centrifuge tests, an evaluation of pile performance depending on the installation method is possible.

The soil state around the wished-in-place piles has not been disturbed by an installation process. In order to mobilise the pile resistance, a large displacement is necessary. This results in the relatively low initial stiffness exhibited in the load–displacement curve of the wished-in-place pile in a loose, cellulose ether saturated sample (T10) compared with the other pile test results. This low initial stiffness can also be seen in Table 3. The low stiffness leads to the wished-in-place pile showing the lowest measured static resistance at 0·05 D_a and at 0·1 D_a, with the exception of T6. Further, even after a displacement of approximately 0·2 D_a no ultimate capacity is evident. This holds true even though the cone resistance at pile tip during the SLT and the averaged cone resistance are comparable to other test scenarios at similar depths (cf. Table 1).

4.2.2 Repeatability of SLT results

The repeatability of the tests can be investigated from the results of two SLTs of an impact-driven pile in loose, dry sand at a depth of 4 D_a (T2, T4). The results are very similar (Figure 7). The initial gradient of the load–displacement curves and the static resistance at a displacement of 0·05 D_a listed in Table 3 are nearly identical for both piles. The measured cone resistance at the final embedment depth of the pile and the cone resistance averaged over depth are slightly different for these cases, with box 2 (T4) having slightly greater cone resistance than box 1 (T2) (cf. Table 1). In spite of this, T4 shows, if anything, a slightly softer response, reflecting the changes in soil density that accompany driving and the greater number of hammer blows applied for T2 than for T4.

4.2.3 Effect of installation method on SLTs in loose sand – jacked pile

The behaviour of the jacked piles (T1, T6, T8) during the SLT is similar to each other. This is depicted in Figures 6 and 8, where the penetration resistance is normalised by the cone tip resistance. The cone tip resistance is considered as the measured CPT data over depth. Hence, for each measurement of the force, the corresponding CPT measurement within the same depth as the force measurement is used for the normalisation. The considered area A is the cross-sectional area of the pile tip. All jacked pile SLTs (T1, T6, T8) show an initially stiff behaviour and then approach an apparent plateau in the load. However, this largely reflects the process of jacking, unloading and then reloading again. This capacity results are much lower values of resistance mobilised at displacements of 0·05 D_a and 0·1 D_a compared with the driven piles, as listed in Table 3. The jacked pile in a water saturated, loose sample (T6) is initially softer and also exhibits a smaller absolute resistance (Figure 6). It is obvious that the measured static mobilised resistances at a displacement of 0·1 D_a and at 0·05 D_a as shown in Table 3 are very similar for the jacked piles in dry (T1) and cellulose ether saturated, loose sand (T8), while the values for the jacked pile in water-saturated sand (T6) vary. While the values for the averaged cone resistance and the cone resistance at pile tip during SLT are very similar for the jacked pile in dry and cellulose ether saturated sand, the cone resistance for the test in water-saturated sand remains well below these values. This box 4, in which T6 was conducted, also had the lowest measured cone tip resistance (Figure 2). The lower measured cone resistance for T6 is also shown in Table 1. The finding is confirmed by the normalisation (Figure 8), which brings the initial response of the three tests closer, although the normalised stiffness for T6 is still the lowest. The normalised capacity of T6, however, is larger than that of the tests in the samples with slightly higher relative sand density (T1, T8).

4.2.4 Effect of installation method on SLTs in loose sand – impact-driven pile

All impact-driven piles retain their high initial stiffness until the actuator capacity was reached in the SLT, such that none of the static measurements for the impact-driven piles reached a displacement of 0·1 D_a.

Assuming the same soil conditions, the load–displacement behaviour of a pile depends greatly on the behaviour of the soil column inside the pile. Different states of plugging will lead to different stiffness of the pile response, even though in early loading the soil plug state is less significant. This is seen for the wished-in-place pile T10, which behaves initially similar to other piles, such as T11 or T9, and then much softer as the soil plug is compressed in order to build end-bearing resistance across the whole pile. Therefore, a reasonable explanation of

Table 3. Overview of the performed test as well as test labels

Test	Soil sample	Pile installation method	Depth of SLT	Static resistance at $0{\cdot}05D_a$	Static resistance at $0{\cdot}1D_a$	Initial gradient at $0{\cdot}002D_a$	Depth of DLT	Soil resistance $j_c = 0$	Soil resistance $j_c = 0{\cdot}5$
T1	Loose, dry (box 1)	Jacked	$2D_a$	35·5 MN	40·1 MN	45 455 MN/m	$2D_a$	5·14 MN	2·03 MN
							$2{\cdot}2D_a$	6·34 MN	2·55 MN
T2	Loose, dry (box 1)	Impact driven	$4D_a$	42·9 MN	NA	45 455 MN/m	$2{\cdot}8D_a$	6·00 MN	3·31 MN
							$4D_a$	9·95 MN	5·95 MN
T3	Loose, dry (box 2)	Wished-in-place	$4{\cdot}6D_a$	NA	NA	NA	$4{\cdot}6D_a$	NA	NA
T4	Loose, dry (box 2)	Impact driven	$4D_a$	41·3 MN	NA	35 714 MN/m	$2{\cdot}8D_a$	5·98 MN	3·52 MN
							$4D_a$	NA	NA
T5	Loose, dry (box 3)	Impact driven	$4{\cdot}4D_a$	NA	NA	13 699 MN/m	$4{\cdot}4D_a$	12·77 MN	9·66 MN
T6	Loose, water saturated (box 4)	Jacked	$1{\cdot}8D_a$	14·9 MN	26·0 MN	7143 MN/m	—	NA	NA
T7	Loose, water saturated (box 4)	Impact driven	$3D_a$	30·5 MN	NA	33 333 MN/m	$3D_a$	6·31 MN	3·01 MN
T8	Loose, cellulose ether saturated (box 5)	Jacked	$2{\cdot}4D_a$	28·3 MN	38·2 MN	12 346 MN/m	$2{\cdot}4D_a$	5·15 MN	2·81 MN
							$2{\cdot}6D_a$	5·05 MN	3·18 MN
T9	Loose, cellulose ether saturated (box 5)	Impact driven	$3{\cdot}4D_a$	31·2 MN	NA	16 949 MN/m	$3D_a$	8·40 MN	5·63 MN
							$3{\cdot}4D_a$	8·63 MN	8·22 MN
T10	Loose, cellulose ether saturated (box 6)	Wished-in-place	$4{\cdot}6D_a$	20·0 MN	32·0 MN	22 727 MN/m	$4{\cdot}6D_a$	1·71 MN	2·21 MN
T11	Loose, cellulose ether saturated (box 6)	Impact driven	$2{\cdot}2D_a$	30·8 MN	NA	20 000 MN/m	$2{\cdot}2D_a$	7·46 MN	5·98 MN
T12	Dense, dry (box 7)	Impact driven	$3{\cdot}1D_a$	39·2 MN	NA	35 714 MN/m	$3{\cdot}1D_a$	9·21 MN	6·17 MN
T13	Dense, water saturated (box 7)	Impact driven	$3D_a$	37·5 MN	NA	71 429 MN/m	$3D_a$	5·26 MN	3·88 MN

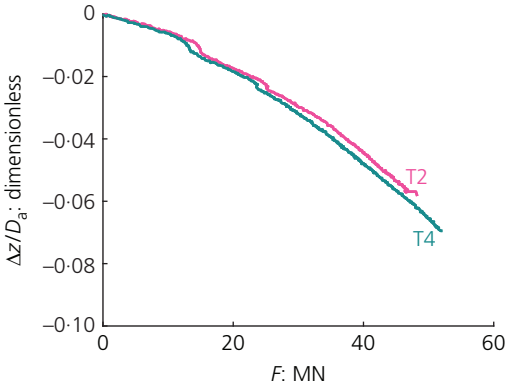

Figure 7. Repeatability of SLT results for the same embedment length in different sand samples

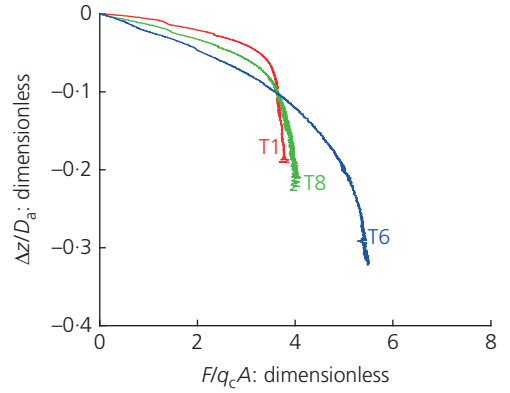

Figure 8. Results of SLT of jacked piles (T1, T6, T8) for varying conditions of saturation of the soil

the difference in behaviour of jacked and impact-driven piles observed from the centrifuge test results is a different state of plugging. All jacked piles should feature a similar state of plugging inside the pile during the performed SLTs, given similar embedment depths for T1 and T6 (with a higher embedment depth for T8), similar initial soil state (as evidenced by similar q_c, see Table 1) and the expected drained installation process. In contrast, densification effects take place within the loose soil for impact driving.

Densification effects enable plugging for the impact-driven piles loose sands. Since no significant effect from densification is expected for the jacked piles in loose sand no plugging is assumed. It has to be noted that the resistance mobilised by the jacked piles reflects the jacking capacity imposed by the actuator limit. The impact-driven pile of T11 has a comparable embedment depth to the jacked piles. The higher measured

soil resistance of T11 compared with the jacked piles may be assumed due to installation effects as densifying the soil and hence increasing external friction. Apart from T11, the impact-driven piles have a greater embedment length than the jacked piles. Opposed to the jacked piles, where the installation depth was determined by the capacity of the actuator, the impact-driven piles could be installed to much greater depth, in spite of the hammer not functioning well. Disregarding this key influence in the prediction method, jacked piles in dependence of the relative density of the soil and the inner pile diameter are expected to show a significantly stronger tendency towards plugging compared with impact-driven piles. Instead, due to densification in the loose sand in the current tests, the impact-driven pile T11 shows a stiffer response when tested statically compared with jacked piles T6 (much lower embedment) and T8 (greater embedment, but surprisingly lower stiffness compared with T1 (slightly lower embedment).

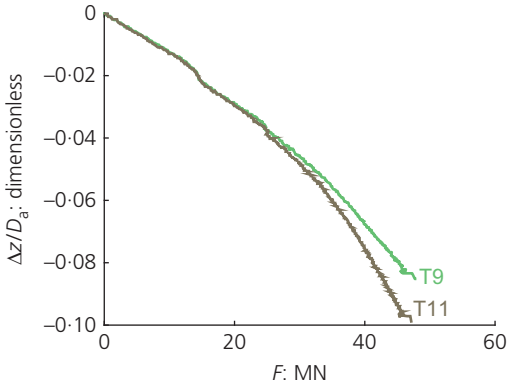

Figure 9. SLT results for different installation depths, impact-driven pile

4.2.5 Influence of installation depth on SLT results

As the embedment depth of the piles after installation differed (Table 1 and Figure 5), it is of interest to explore the influence of the installation depth on the SLT results.

Differences in response due to the installation depth can be evaluated for impact-driven piles installed in cellulose ether saturated, loose sand samples. The driven pile of T9 had an embedment depth of $3{\cdot}4D_a$, while T11 was driven to a depth of $2{\cdot}2D_a$. The measured cone resistance at the tip of the pile at the final installation depth and the averaged cone resistance, as listed in Table 1, are comparable but not identical for these two cases. Even though the increase in embedment depth is noticeable within the SLT measurements and the cone resistance the study of the influence of the installation depth on SLT results is possible. The SLT results for these two cases are illustrated in Figure 9.

The load–displacement curves are almost indistinguishable initially but start to diverge at a normalised displacement $\Delta z/D_a = -0{\cdot}04$. The initial gradient listed in Table 3 is similar for both tests and the static resistance mobilised at a displacement of $0{\cdot}05\ D_a$ differs only marginally. Inspection of the piles following extraction after the centrifuge tests showed highly densified and compacted soil plug, suggesting that the static response was fully plugged for both piles. Therefore, the slight divergence of the loading responses at higher loads reflects small differences in the shaft friction and end bearing as a result of the greater installation depth for T9.

A general tendency of increasing static resistance mobilised at a pile displacement of $0{\cdot}05D_a$ with increasing embedment depth can be observed for all piles within all variations. However, there is also a significant dependency between saturation of the soil and measured resistance especially for the impact-driven piles as well as a dependency between installation method and static resistance mobilised within the data listed in Table 3.

4.2.6 Influence of pore fluid response on SLT results

Besides the installation method, saturation of the soil is an essential characteristic, which was varied during these centrifuge tests. While this is not expected to influence the jacked piles due to the chosen installation rate and the resulting drained response, the pore fluid response may have influenced the soil state as vertical effective stress profile around the impact-driven piles, even if any excess pore pressures arising from the installation were allowed to dissipate prior to the SLT (which itself is expected to be drained given the low displacement rate). In order to evaluate this effect, Figure 10 illustrates the absolute and normalised measured responses for impact-driven piles in dry loose soil (T2), in water-saturated soil (T7) and in cellulose ether saturated loose soil (T9).

The piles in T2, T7 and T9 were installed to different embedment depths. A difference in the measured cone resistances at the pile tip position after installation, summarised in Table 1, can be seen. Hence, the depicted measurement results include a difference in inner and outer skin friction along the pile shaft. However, the difference in installation depth is smaller than for the differences in embedment depth for the evaluation in the previous section for T9 and T11. Despite this, the load–displacement curves of T2, T7 and T9 show more significant differences, potentially reflecting of effects of the different pore fluids.

The SLT responses for T2 (dry soil) and T9 (cellulose ether saturated sample) are of similar shape (Figure 10(a)), but with T2 showing significantly greater initial stiffness and resistance

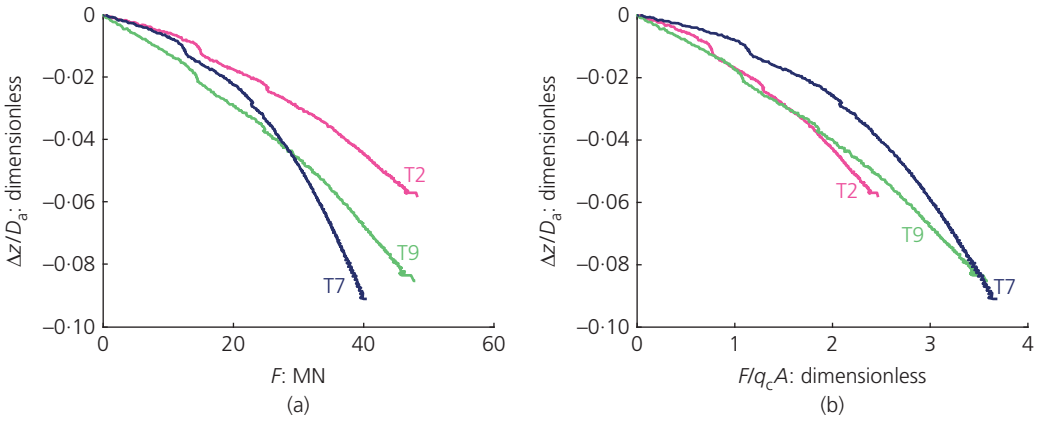

Figure 10. (a, b) Results of SLT of impact-driven piles for varying conditions of saturation of the soil

at a displacement of $0{\cdot}05D_a$ (Table 3). The response for T7 (water-saturated sample), with the shallowest embedment, shows much greater curvature. The initial stiffness is similar to that for T2, but the resistance mobilised is similar to T9 at a displacement of $0{\cdot}05D_a$ and then lower thereafter. The results for the static resistance at a displacement of $0{\cdot}05$ D_a in Table 3 reveal that those for piles within the fluid-saturated samples are nearly identical, while corresponding values for the impact-driven piles in dry sand are higher. This holds true for all performed tests.

Normalising the resistances according to the cone tip resistances brings the T2 and T9 SLT responses together (Figure 10(b)), while that for T7 is initially much stiffer than either. The greater curvature in the T7 response brings the curves gradually together so that it shows similar normalised resistance to T9 at a displacement of about $0{\cdot}1D_a$. Hence, it might be that the difference occurs due to different states of plugging induced by the pore fluid response during the installation process. A partially plugged pile will respond softer initially than a fully plugged pile but with sufficient additional penetration depth might eventually converge to a similar normalised ultimate load. It might be possible that the shallowest test T7, while stiff initially, shows lower resistance mobilised as a result of partial plugging during static loading.

4.2.7 Influence of relative density on SLT results

SLT results for an impact-driven pile in dry and water-saturated, dense sand (T12 and T13) were obtained from the performed centrifuge tests. Therefore, an evaluation of the influence of the relative density on SLT results can be conducted for impact-driven piles only. The results as measured force F against normalised displacement $\Delta z/D_a$ are shown in Figure 11. Just as for the loose sand, saturation of the soil, hence reducing the vertical effective stress and cone resistance, reduces the axial capacity of the pile. However, while the initial gradient is significantly larger for the pile in water-saturated dense sand, the static resistance mobilised at $0{\cdot}05$ D_a for both piles T12 and T13 in the dense sample are very similar, as shown in Table 3. The impact-driven pile in loose, water-saturated soil (T7) has the same final embedment length as the impact-driven pile in dense water-saturated sand (T13). Due to higher shaft friction and tip pressure, the static resistance of the pile installed in dense sand is significantly greater than for the pile in loose sand (cf. Table 3). However, up to a pile displacement of approximately $0{\cdot}02D_a$, the SLT response of both piles is surprisingly similar in spite of the different CPT profiles. Indeed, the normalised responses in Figure 11(b) show much greater (normalised) resistances mobilised for T7. A possible explanation is that the large number of blows required to install the piles has partially obliterated the effect of the initial difference in density. In the later part of the tests, the soil resistance mobilised by the pile in dense sand, T13, becomes significantly greater than that for T7 in loose sand, but the difference is still much less than the six- to nine-fold difference in CPT resistance.

In contrast to the piles in saturated sand (T7 and T13), the measured force during the SLT on the impact-driven pile in dense, dry sand (T12) is lower than that for the impact-driven piles in loose, dry sand (T2) throughout the test. This may be attributed partly to the difference in embedment lengths of $1{\cdot}0D_a$, although the T2 response is still surprisingly stiff. The larger shaft friction and tip resistance in the dense sand should lead to a higher bearing capacity when installed to the same embedment depth. However, the state of plugging influences this greatly. In dense sand, the tests T12 (dry sand) and T13 (water-saturated sand) are pretty similar with, as expected, very slightly greater absolute resistances from T12 (dry sand).

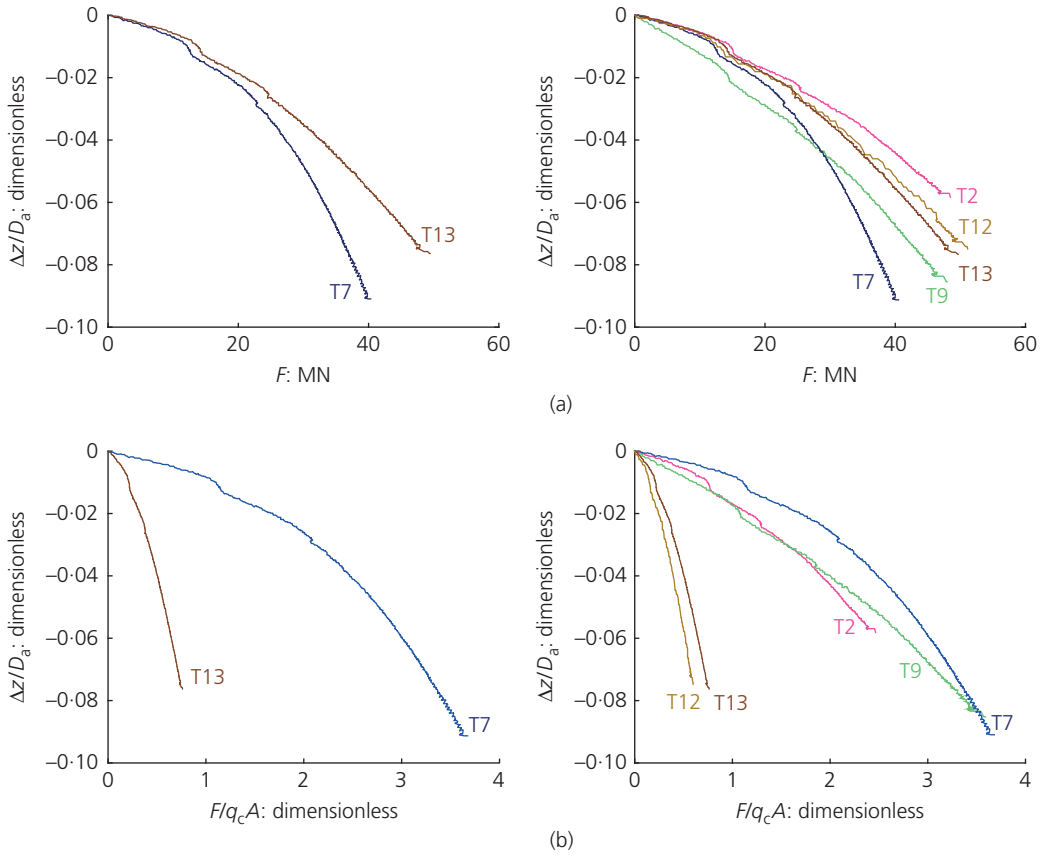

Figure 11. (a, b) Results of SLT of impact-driven piles for varying initial relative densities and saturation of the soil

For T2 (loose, dry sand) and T9 (loose, cellulose ether saturated sand), the difference appears to be consistent with the difference in CPT resistance. Therefore, the saturation influences the SLT results as far as the CPT resistance drops for the saturated samples. It is not clear, however, if the different drainage characteristics between water and cellulose ether saturation has much effect.

4.2.8 Summary of SLT findings

The following synthesis summarises the SLT results of this centrifuge testing programme on large-diameter piles

- The installation method affects both the stiffness and the ultimate capacity of the pile.
- SLT results were shown to be repeatable.
- The installation depth affects the SLT results of impact-driven piles.
- The pore fluid response influences the results of impact-driven piles, even if excess pore pressures are allowed to dissipate prior to the SLT, through differences in the installation induced soil state inside and around the pile due to the pore fluid response.
- The initial sand relative density has an impact on the bearing capacity of the tested piles, as expected, although by a lesser margin than differences in cone tip resistance would suggest.

4.3 Dynamic load tests

DLTs were conducted at the same embedment depth just prior to the SLTs discussed above. An overview of the DLTs performed, differentiated by installation method, relative density of the soil, saturation of the soil and embedment depth of the pile is given in Table 1 and Figure 5.

Example pile head signals obtained from a DLT on a large-diameter open-ended pile are shown in Figure 12. The results of the stress wave velocity inside the pile are taken from the Hopkinson bar measurements. The accelerometer measurements were influenced by resonance effects and oscillations, are deemed unreliable and are hence discarded. The results of

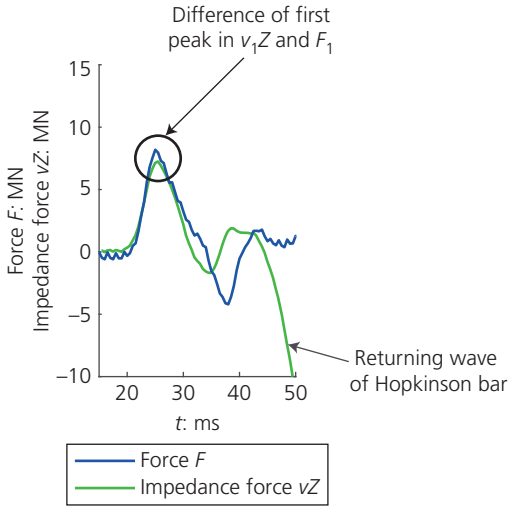

Figure 12. Example of DLT results in loose, dry sand (T1) at $z/D_a = 2$

the Hopkinson bar are valid until the returning wave inside the PVC strip reaches the strain gauges and influences the measurement of the velocity at pile head. This occurs beyond about 42 ms. The large decrease in the impedance force vZ characterises this point in the measurement curve.

The example curve shows the derived force F and impedance force vZ over time of a DLT on a jacked pile in loose, dry sand (T1) at an embedment depth of $2D_a$. Both curves rise with the same slope until the peak of the wave propagates past the measurement devices (at approximately 25 ms). The pile head signals reveal a slight difference between force F and impedance force vZ for the first peak. The reason for this difference is an upwards travelling wave caused by the reflection of the initial wave along the pile shaft due to shaft friction. This first part of the wave is reflected below the soil surface and returns to the measurement level before the peak of the initial wave has travelled past the instrumentation and hence affects the initial peak. Post peak, F and vZ curves decreases together, but with $F > vZ$ due to cumulative reflections from shaft friction until the returning wave from the pile tip passes the sensors again at approximately 37·2 ms. At that stage F decreases more sharply, becoming tensile, while vZ increases, both of which imply a tension wave has travelled through the pile from the tip to head as a result of low resistance mobilised at the pile tip. Shortly after the returning wave is detected (at ∼37·2 ms) the return wave of the Hopkinson bar becomes obvious within the impedance curve measurement (at ∼42 ms).

The value of the maximum measured force F is smaller than expected. On the basis of a 50 g mass and a drop height of 17 mm (model scale), an impact force of approximately 50–100 MN at prototype scale was expected. This compares with measured maximum values in the range 4–10 MN. Also, it is generally assumed that the maximum impact force needs to exceed the soil resistance in order to achieve acceptable driving. Here, the piles were driven successfully (albeit with very high blow counts) to penetrations at which the pile capacity was well in excess of 40 MN, so a factor 4–10 greater than the maximum impact force. Investigations following the centrifuge tests revealed that the driving hammer was not functioning well due to an inadequate air supply. Hence, the maximum force was limited to approximately 10 MN and with a rather variable force between tests, averaging 8 MN but in one case as low as 4 MN.

Although malfunctioning of the driving hammer limited the resistances mobilised during the DLTs to well below those from the SLTs it is still possible to comment on variations between different DLTs. Detailed stress-wave interpretation is not presented here. However, in addition to comparison of the curves of force F and impedance force vZ directly the DLT measurements have been evaluated using the standard CASE method in order to estimate total and (nominally) static soil resistance mobilised in each test. The mobilised soil resistance SR is computed from continuous F and vZ curves from the CASE formula

$$\text{SR} = 0{\cdot}5(1-j_c)(F+Zv)_{t=t-2L/c} + 0{\cdot}5(1+j_c)(F-Zv)_{t=t} \quad (5)$$

where j_c is the case damping factor and L symbolises the length between sensor and pile tip. The total mobilised soil resistance is calculated by using a damping factor of $j_c = 0$, while the static resistance based on a damping factor of $j_c = 0{\cdot}5$. The results for the total and the static mobilised soil resistance for each test are summarised in Table 3. No data are available for T6 since no DLT was performed, for T4 because the force signal was corrupted and for T3, where the SLT and DLT data suggest a missing tip support and unreliable measured responses. The evaluation using the CASE method for tests T4, T7 and T12 have to be treated with caution since these tests have a poor initial proportionality between force F and impedance force vZ. For the example curve shown above, a mobilised static resistance of SR = 2·03 MN and a total soil resistance of SR = 5·14 MN are derived.

4.3.1 Repeatability of DLT results

To compare the results of DLTs on piles in different soil samples, the repeatability of the results is first evaluated. DLTs on an impact-driven pile in loose, dry sand are available at embedment lengths of $2{\cdot}8D_a$ and $4D_a$ in two soil samples (T2, T4). These four results can be compared in order to assess the repeatability of the dynamic tests. The cone resistances at the pile tip at the final installation depth and averaged over depth

is listed for these cases in Table 1. The cone resistance for T4 is higher than for T2, which must be borne in mind in comparing the DLT results.

The pile head signals are shown in Figure 13. (The strain gauge measurement in T4 was (mechanically) disturbed after the first peak and the remainder has been discounted.) As for the SLTs, the results of the DLTs are very similar but not identical for equivalent cases. The results for the deduced soil resistance provide similar evidence. The total resistance determined for T2 and T4 at an embedment depth of $2{\cdot}8D_a$ is SR = 6·0 MN. The static soil resistance varies between SR = 3·31 MN for T2 and SR = 3·52 MN for T4 at a depth of $2{\cdot}8D_a$. This difference of about 6% in the mobilised static soil resistance most probably results from the minor difference in the soil samples as characterised by the CPT profiles in Figure 2 and by the values for the cone resistance listed in Table 1. Interestingly, though, the difference is the reverse compared with the SLTs on T2 and T4, where T4 should slightly lower resistance. Overall, repeatability of the dynamic test results appears reasonable.

4.3.2 Influence of installation depth on DLT results

The effect of pile installation depth on DLT results can be evaluated through comparison of the following results shown in Figures 14 and 15

- A jacked pile in a dry, loose sample (T1) at an embedment length of $2D_a$ and $2{\cdot}2D_a$, respectively.
- A jacked pile in a cellulose ether saturated, loose sample (T8) at an embedment length of $2{\cdot}4D_a$ and $2{\cdot}6D_a$, respectively.
- Two impact-driven piles in dry, loose samples (T2, T4) at an installation depth of $2{\cdot}8D_a$ and $4D_a$, respectively.

The difference in the pile head signals of T1 due to shaft friction is small at $z/D_a = 2$, as discussed earlier (Figure 12). A larger embedment length decreases the distance between measurement level and ground surface. Therefore, further reflections can reach the sensors before the first peak is registered, and the influence of shaft friction on pile head signals increases. This manifests itself as an increase in peak difference with increasing embedment depth.

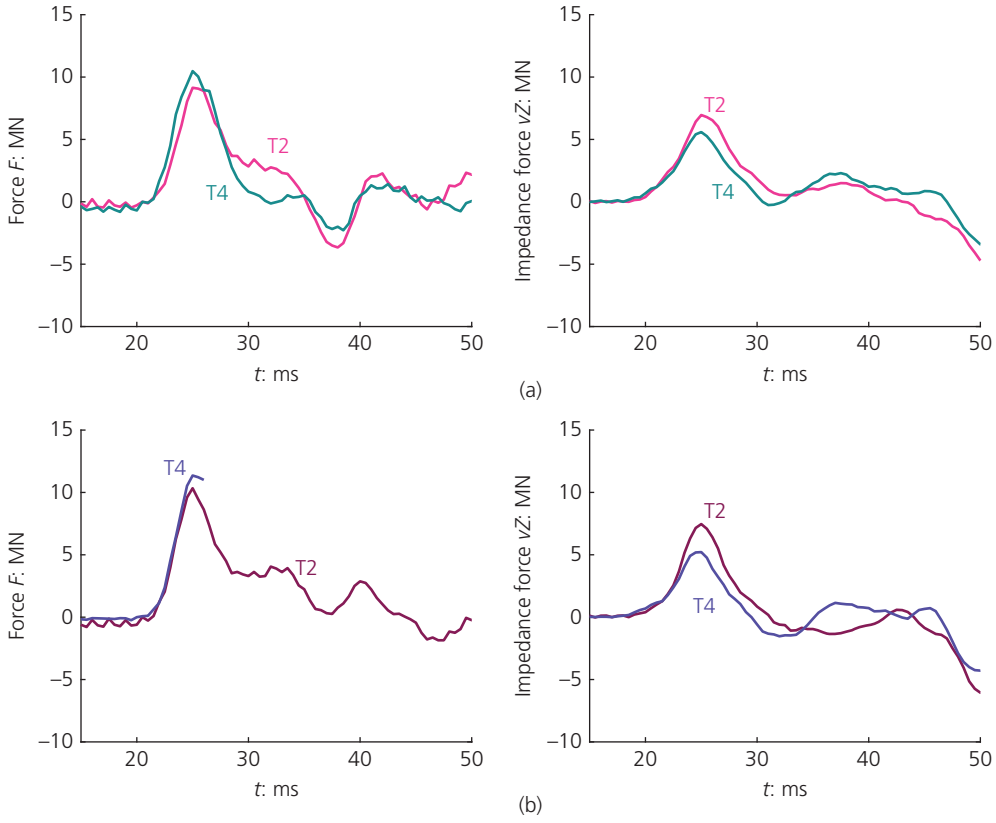

Figure 13. DLT results for the same embedment length in different samples, (a) $L_e = 2{\cdot}8\ D_a$ (b) $L_e = 4\ D_a$

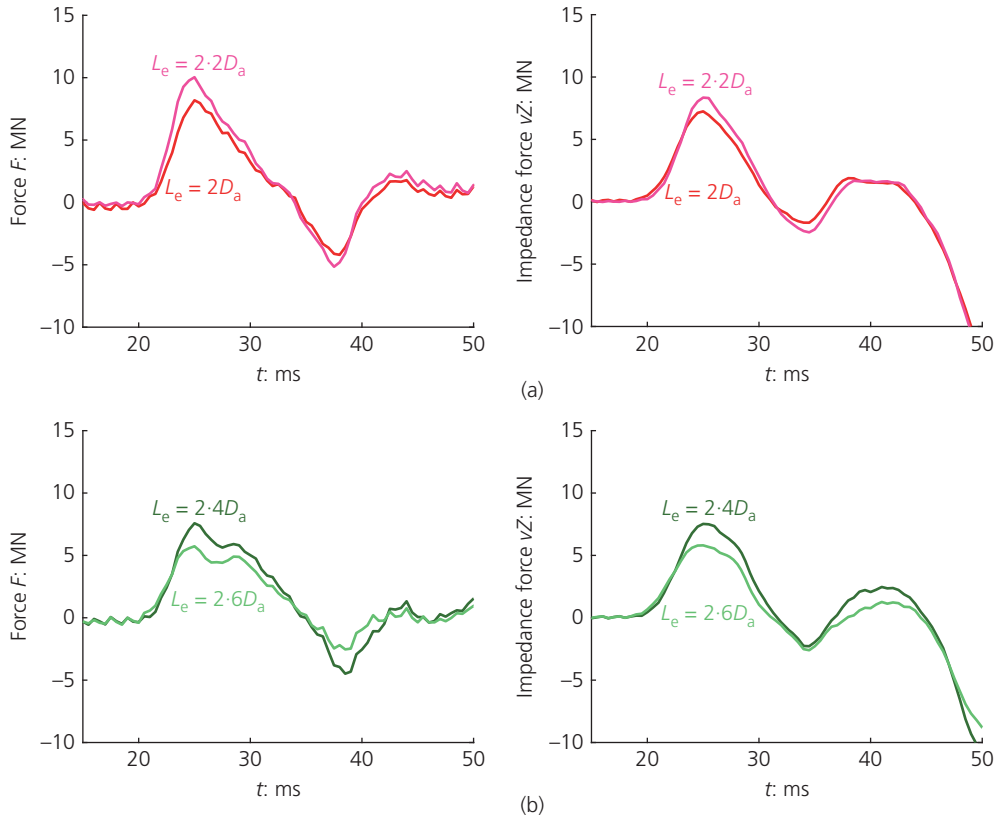

Figure 14. DLT results at different embedment depths for two jacked piles, (a) T1, (b) T8

When comparing the force F and impedance force vZ at two embedment depths for the same pile, the results for both T1 and T8 are comparable. For T1 the deeper DLT shows increased values for F and vZ at t_1 and t_2, while the reverse is true for T8. This might be due to the random variation in impact force due to poor air supply. For both piles, the deduced static mobilised soil resistance shows a small increase with increasing embedment depth (cf. Table 3). The rather small difference is consistent with the small increase in installation depth.

The difference in installation depth, $1{\cdot}2D_a$, for the impact-driven piles, T2 and T4, is greater than for the jacked piles (Figure 15). The main difference in the pile head signals of the impact-driven piles lies in the return wave. In T2 and T4, the first DLT at a depth of $2{\cdot}8D_a$ shows the characteristics of a low tip resistance, whereas the second DLT on this pile starts to reveal increased tip resistance for the pile with the signals showing a returning tension wave for the first DLT and a returning compression wave for the second DLT. The derived total soil resistance for T2 listed in Table 3 varies from SR = 6·0 MN for an embedment depth of $2{\cdot}8D_a$ to SR = 9·95 MN for the greater embedment depth of $4D_a$. The corresponding mobilised static soil resistance increases from SR = 3·31 MN for $2{\cdot}8D_a$ to SR = 5·95 MN at $4D_a$. The increase in static mobilised resistance with increasing embedment deduced from the DLTs is consistent with observations from the SLTs, for example in the increase in resistance mobilised at a displacement of $0{\cdot}05D_a$ between T11 (embedment of $2{\cdot}2D_a$) and SLTs on impact-driven piles at greater embedment.

4.3.3 Comparison of DLT results on impact-driven piles

Within each soil sample, an impact-driven pile was tested dynamically. Therefore, more than one set of measured DLT data exists on impact-driven piles in both dry, loose sand and cellulose ether saturated, loose sand. Figure 16 summarises these results by depicting force F and impedance force vZ over time.

The final embedment depth for all impact-driven piles in loose, dry soil (T2, T4 and T5) is approximately $4D_a$. The values for the cone resistance at the pile tip and the averaged cone resistance, as summarised in Table 1, show some variation among these three tests, with T4 having slightly higher cone resistance. Comparing the results of T2, T4 and T5 reveals that the force F response is comparable while the impedance force

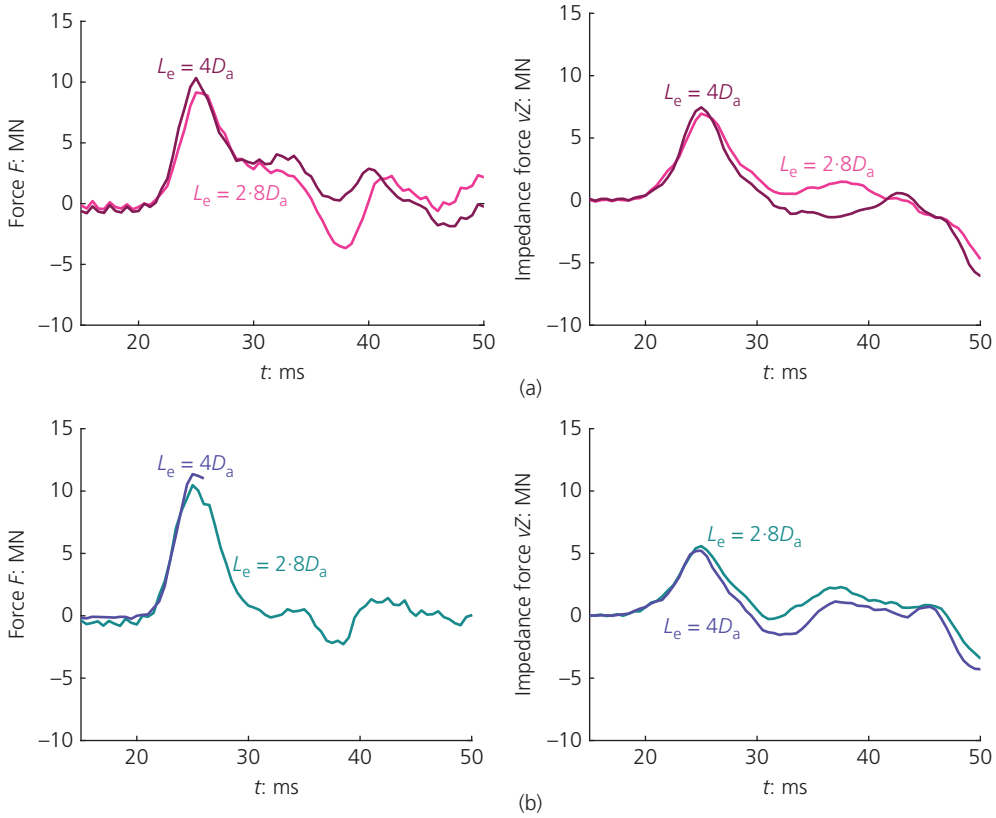

Figure 15. DLT results at different embedment depths for two impact-driven piles, (a) T2, (b) T4

vZ shows a decreasing initial peak from T5 to T4. All responses suggest mobilisation of significant tip resistances, especially for T5. Comparison of the mobilised resistance evaluated from the DLT measurements using the CASE method at this considered embedment depth is only possible for T5 and T2. As shown in Table 3 both the total and the static mobilised soil resistance reveal significantly higher values for T5 compared with T2, with the mobilised static resistance for T5 being the highest among all the piles tested. The initial stiffness of T5 during the SLT is the lowest for all impact-driven piles. However, the resistance mobilised cannot be deduced from the SLT data because the limit of the load cell was reached before a sufficient pile displacement was reached.

The relative density of the cellulose ether saturated sample for box 6 (T10 and T11) was slightly greater than for box 5 (T8 and T9) due to the difficulties in sample preparation with the wished-in-place pile present (cf. Figure 2), which also causes a difference within the measured cone resistances shown in Table 1. Due to that, and also likely less good performance of the hammer for T11 (noting the lower maximum force level), the maximum embedment depth achieved for the impact-driven pile of T11 was only $2{\cdot}2D_a$ compared with $3{\cdot}4D_a$ for T9. Comparing the pile head signals of T11 with DLT results for both testing depths of T9 reveals that all curves are quite similar, although with T11 showing lower maximum dynamic force, and suggest relatively high tip resistance for all three tests. The force F and impedance force vZ of T9 at the smaller embedment depth are larger than for the other tests. Additionally, as shown in Table 3, the derived soil resistances, total and static, are similar for both T9 DLTs and T11, although the mobilised static soil resistance for the deeper DLT on T9 is the largest, perhaps reflecting the greater embedment depth. The results of T9 are used below for comparison of DLTs on piles with different pore fluids.

4.3.4 Influence of relative density on DLT results

The impact-driven pile in dense, dry sand (T12) was tested dynamically at an installation depth of $3{\cdot}1D_a$. In order to compare this result with a dynamic pile test on an impact-driven pile in loose sand (T2) testing depths of $2{\cdot}8D_a$ or $4{\cdot}0D_a$ can be chosen. The results for these three DLTs are illustrated by force F and impedance force vZ over time in Figure 17. The DLT on the pile in dense sand (T12) reflects mobilisation of high tip resistance, which corresponds to the significantly higher cone resistance throughout the dense sample. The

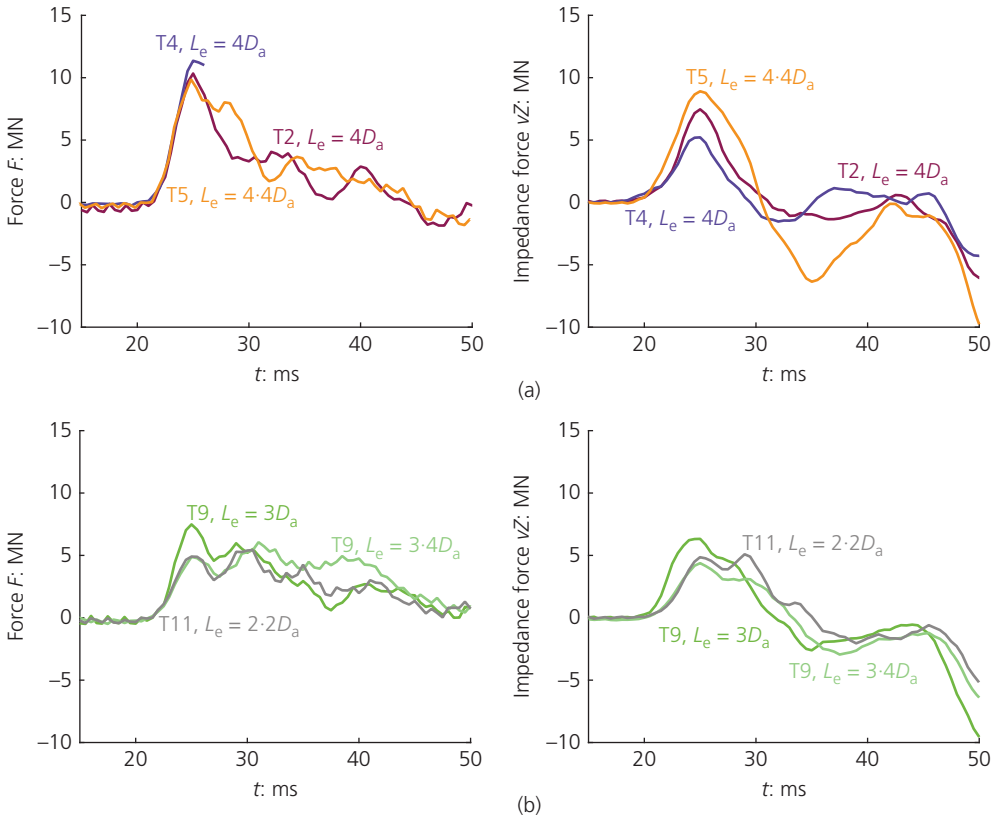

Figure 16. Comparison of DLT results on impact-driven piles in (a) loose, dry and (b) loose, cellulose ether saturated sand

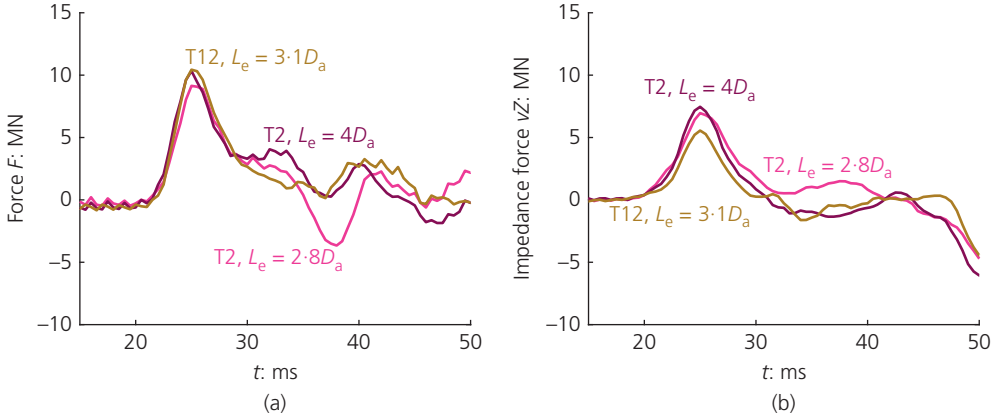

Figure 17. (a, b) DLT results for a variation the relative density of the soil sample

resulting return wave is comparable to the dynamic pile test on the pile in the loose soil (T2) with an embedment length of $4{\cdot}0D_a$. The DLT on the same pile at shallower embedment shows the behaviour of a pile with low tip resistance hence reflection of a tensile force wave. The similarity in the measured force F for both T12 and the deeper DLT T2 shows that the dynamic pile responses are essentially independent of the initial relative density of the soil and the cone resistance of the soil, as noted previously for the corresponding SLTs. The maximum impedance force vZ for the pile in dense sand (T12)

is smaller than for both DLTs in T2 in loose sand. This suggests greater shaft friction in dense sand in comparison to loose sand, consistent with the much greater cone resistance.

The mobilised static soil resistance is very similar for the deeper DLT on T2 and T12, while it is smaller for the shallower DLT on T2 (SR = 3·31 MN compared with the other two cases (T2, $4D_a$: SR = 5·95 MN and T12: SR = 6·17 MN)). Again this is consistent with the measured SLT responses suggesting that the relative density did not have a significant influence on the static soil resistance mobilised at displacements up to $0{\cdot}05D_a$. Essentially, it is as if pile installation has locally obliterated the large difference in initial relative density and cone resistance in these two samples.

4.3.5 Influence of pore fluid response on DLT results

A fundamental difference between the soil samples is the saturation. The measured pile head signals for an impact-driven pile in dry (T2), water-saturated (T7) and cellulose ether saturated (T9) loose sand, and dry (T12) and water-saturated (T13) dense sand are shown in Figure 18.

In loose sand, the peak values of the force F and impedance force vZ are largest for the DLT on an impact-driven pile in dry soil (T2) and in water-saturated sand (T7). The results of the T7 DLT should be treated with circumspection. In loose, dry sand (T2), the form of the stress wave suggests low tip resistance, which is reflected in the low mobilised resistances tabulated in Table 3. By contrast in the cellulose ether saturated sand (T9) the stress waves suggest much higher tip resistance, consistent with the higher mobilised soil resistance even though the embedment depths for T2 (for the shallower DLT) and T9 are quite similar.

In dense sand, high resistance is developed at the pile tip for both dry (T12) and water-saturated (T13) conditions. Hence, a comparison of the starting and the return wave is possible. The initial wave is significantly stronger for a DLT on a pile in dry sand in comparison to a pile in saturated soil, implying higher shaft friction. The measured CPT data as listed in Table 1 reveal higher cone resistances at the depth of the final pile position and averaged over depth for the dry cases in comparison to the saturated soil samples. Consequently, the difference in value of the first peak between force F and impedance force vZ differs because the skin friction differs. The measurements of both piles tested in dense sand remain similar for the return wave and do not show great discrepancies. However, this evaluation needs to be considered with caution since a malfunction of the hammer can have occurred for T13 showing the lowest maximum force of any of the tests.

The saturation of the soil and the excess pore-pressure development therefore influence the pile head signals of DLTs. A conclusion, especially for the loose sand, is the ability for the pile to be installed to greater embedment depths in dry loose sand (even with a poorly performing hammer), while for the water-saturated and cellulose ether saturated tests the maximum embedment was much reduced. In addition, on subsequent extraction, the soil plug for the saturated tests was found to be extremely well compacted and difficult to remove from the pile.

The conclusions drawn above can be extended by the study of the derived soil resistances listed in Table 3. The derived total soil resistance is with approximately SR = 9 MN comparable for all cases. Exclusions are the DLT of T2 for the low embedment depth of $2{\cdot}8D_a$ and the DLTs on the pile in water-saturated samples of T7 and T13, which lead to a soil resistance of approximately SR = 6 MN. The deduced static soil resistance shows significant differences. The DLTs on a pile in dry sand (T2 and T12) show greater static soil resistances and measured cone resistances compared with the static soil resistance developed for water-saturated soils (T7 and T13). The static soil resistance of the test T9, where a pile is tested within loose, cellulose ether saturated soil, reveals the largest mobilised static soil resistance. Therefore, the excess pore-water pressure development during a DLT influences the pile head signals and the derived static soil resistance, while a defined classification of the influence cannot be drawn.

4.3.6 Influence of installation method on DLT results

The results of the DLTs of piles installed by jacking, impact driving and no installation (wished-in-place) are plotted in Figure 19. A stiff pile tip support has developed in the impact-driven pile tests at their final installation depth (T9), whereas the jacked and wished-in-place piles (T8, T10) show the characteristics of low mobilised pile tip resistance. This supports the observation in the SLT results that the impact-driven piles behave stiffer during the static tests than the jacked and wished-in-place piles because less densification of the soil plug occurred for the latter piles in contrast to the impact-driven piles. This is the case since the tests are performed in loose sand. Densification due to driving, rather than monotonic compression during jacking, might lead to a greater mobilisation of a soil plug resistance. Generally this would be expected for jacking. This is also supported by the static soil resistance determined as shown in Table 3.

Even though the results of the SLT show a comparably low static resistance mobilised for the wished-in-place pile T10 and in spite of higher cone resistance (cf. Table 1) the static soil resistance derived from the DLT is comparable with that for the jacked pile T1. The derived static soil resistance in the DLT is about SR = 2·21 MN for the wished-in place pile (T10) and SR = 3·18 MN for the jacked pile (T8), while it is

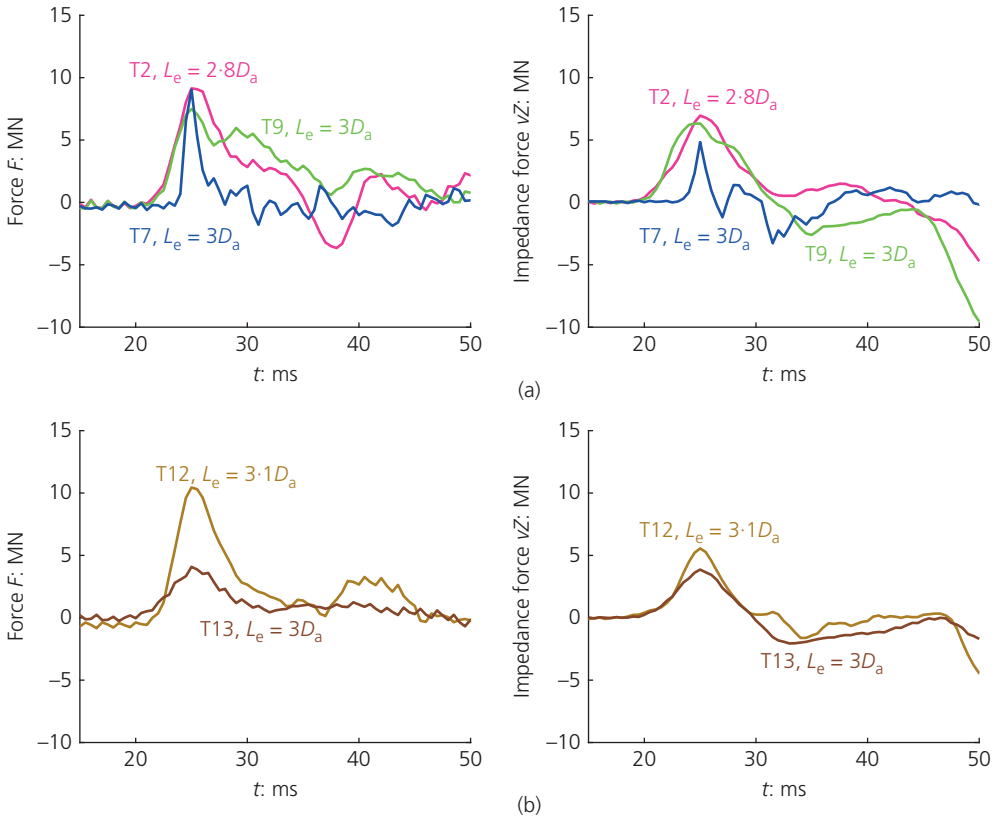

Figure 18. Influence of pore fluid response on DLT signals, (a) loose sand, (b) dense sand

increased to over SR = 8 MN for the impact-driven pile (T9). The calculated total soil resistance shows the same trend.

The DLTs on the piles with low mobilised tip resistance (T8, T10) show a clear tensile force reflection from the pile tip together with increased impedance force. The DLT static soil resistances mobilised for jacked piles (T1 and T8) are similar, within 10%, which is consistent with the results of the SLTs and the measured cone resistances listed in Table 1, which are very similar for the samples T1 and T8. The jacked piles show a relatively low static resistance from DLT in spite of the high maximum loads during SLTs. A possible explanation for this might be a change of mechanism from a quasi-plugged response during SLT to an open-ended failure mode during DLT. The DLT on the wished-in-place pile reveals the largest extreme values within the pile head signals while showing the smallest derived mobilised soil resistance and the DLT on the impact-driven pile has the lowest extreme values within the pile head signals as well as the largest calculated mobilised static soil resistance, while the cone resistances of the impact-driven pile (T9) are due to the greater embedment depth higher than for the jacked pile.

To compare pile head signals for different installation techniques with the same apparent mobilised tip resistance, as judged from the shape of the reflected stress waves, DLTs on jacked and impact-driven piles in the same dry, loose sample (T1, T2) are compared in Figure 19. The shapes of the stress waves are extremely similar, although the mobilised static resistance from T2, while still quite low, is more than 50% greater than for T1. Hence, the DLT measurements at the pile head do not reflect the soil state but primarily the pile tip support. This explains the similarities between the DLT results on the wished-in-place pile (no installation history, T10) and the jacked pile (T8), where the installation should affect the soil state. A significant difference is expected, but is not visible.

The results of this comparison of the DLT results suggest that the DLT is strongly influenced by the pile–soil interaction especially on the inside of the pile (i.e. the state of plugging and hence the pile tip support) but less so by the state of the soil. This goes along with the assumption of a change in mechanism during SLT and DLT as stated above, which is based on the low-resistance mobilised during DLT and the high

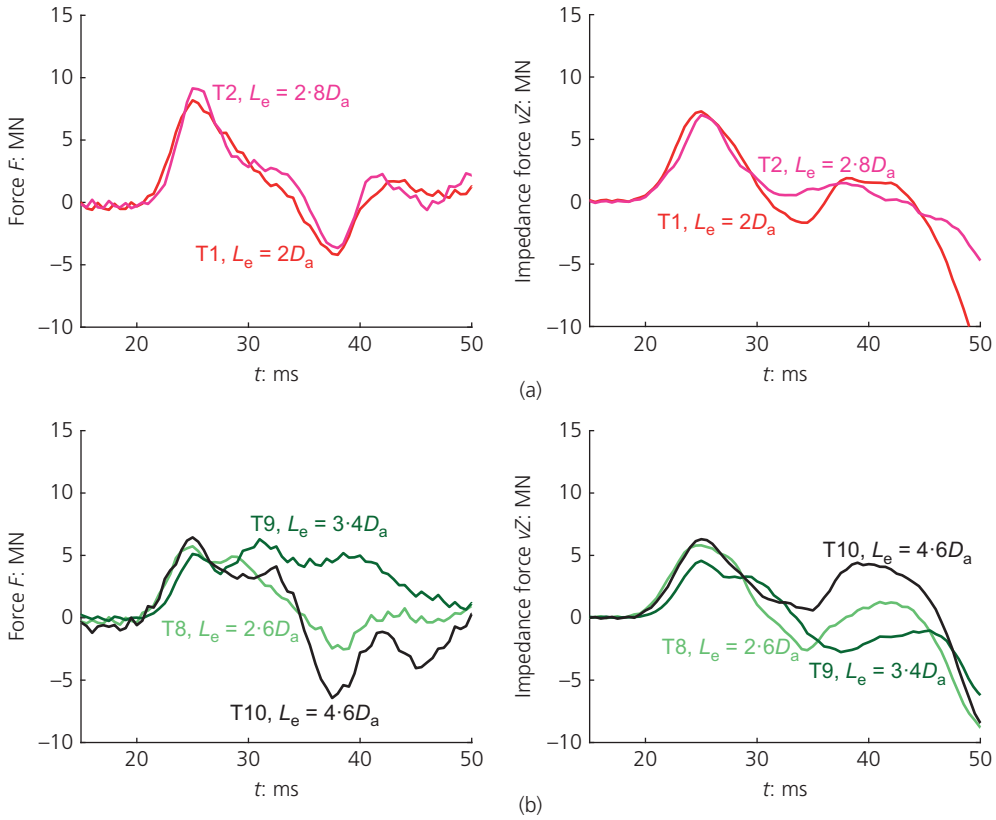

Figure 19. DLT results for varying installation methods in (a) dry and (b) cellulose ether saturated loose sand

measured resistances during SLT for the jacked piles. This finding is expected to hold also for other embedment depths (based on numerical results by Grabe and Heins (2016)) but should be further validated experimentally by physical data.

5. Evaluation of dynamic and SLT results

The results of the centrifuge tests have allowed the evaluation of DLTs and SLTs on the same pile at the same depth. The analyses performed throughout this paper reveal that the results of SLTs are influenced by all parameters considered. Therefore, a distinctive difference between the axial capacity of the installed piles depending on the installation method, installation depth, saturation as well as drainage condition of the soil and sand relative density is observed. The results of the DLTs are influenced by the malfunctioning hammer such that a limited force was applied to the pile. The pile head signals obtained from DLTs in this series of centrifuge tests identify pile–soil interaction (specifically pile tip support) and saturation to be the key influences. Therefore, the static axial pile bearing capacity may differ significantly (as evident from the SLTs) even if the pile head signals obtained from DLTs are similar.

The derived soil resistance based on the CASE method can be compared with the results of the performed SLTs. The soil resistance mobilised in the DLTs performed is with approximately 6–9 MN much lower than the static resistance of the pile determined from SLTs at 0·05 D_a (28–43 MN). The low determined soil resistance from DLTs could be caused by the insufficient energy from the driving hammer. The limited force and pile displacement caused by the hammer blow during DLT might be too low to predict the same resistance as mobilised during SLT. Hence, this evaluation has to be considered carefully.

The DLT results of the performed centrifuge tests can be used to verify assumptions made for the SLT results. The wished-in-place pile neglects installation effects and an unplugged penetration is assumed. A soft pile tip support is assumed for the wished-in-place pile from DLTs and comparable with the low derived static soil resistance from SLTs. The jacked piles were only installed until the load limit of the actuator was approached, which influences the SLT measurements greatly since a re-loading is established by the SLT. A plugged penetration is unlikely to have occurred for the jacked piles. This is

also suggested by the DLT data suggesting a soft pile tip support. The pile behaviour of the jacked piles during SLT is softer than for the impact-driven piles. The evaluation using the CASE formula also suggests smaller mobilised static soil resistances for the jacked piles in comparison with the impact-driven piles. Results of DLTs on impact-driven piles suggest a stiff pile tip support. This explains the stiffer behaviour under static axial loading (as evident in the SLTs) of the impact-driven piles.

6. Conclusions

Centrifuge tests were carried out in order to gain a better understanding of DLTs on large-diameter open-ended piles. To reach this goal a prototype pile with a diameter of $D_a = 5{\cdot}0$ m was installed into sand and at its final installation depth tested dynamically and statically (SLT) in the centrifuge. Effects of the installation method, saturation of the soil and sand relative density were investigated.

The evaluation highlights that the results of the centrifuge tests for DLTs and SLTs are reproducible and can also be compared at slightly different installation depths.

The results of the performed variations confirm that the static axial bearing capacity of open-ended piles in compression as obtained from SLTs depends on the installation method, saturation and sand relative density. The centrifuge test results suggest that the same does not hold for pile head signals of DLTs, with installation depth, installation technique and relative density of the soil not significantly affecting the measurements, unless the pile tip support is influenced. The pile–soil interaction and, in particular, the pile tip support (i.e. free or fixed end) determines the shape and the value of the pile head signals. The drainage conditions were also found to be important influences on the DLT measurements.

Therefore, care has to be taken when evaluating DLT results to derive the static pile bearing capacity as not all factors influencing the static capacity directly manifest themselves in the dynamic pile head signals.

REFERENCES

Abdoun T, Gonzalez MA, Thevanayagam S *et al.* (2003) Centrifuge and large-scale modeling of seismic pore pressures in sand. *Journal of Geotechnical and Geoenvironmental Engineering* **129(12)**: 1083–1091.

Andersen KH, Allard MA and Hermstad J (1994) Centrifuge model tests of a gravity platform on very dense sand, II: interpretation. In *Proceedings of the 7th International Conference on Behavior of Offshore Structures, BOSS 94, Cambridge, MA, USA* (Chryssostomidis C (ed.)). Massachusetts Institute of Technology, Cambridge, MA, USA, vol. 1, pp. 255–282.

Bienen B, Klinkvort RT, O'Loughlin C, Zhu F and Byrne BW (2018) Suction caissons in dense sand, Part I: Installation, limiting capacity and drainage. *Géotechnique* **68(11)**: 937–952, https://doi.org/10.1680/jgeot.16.p.281.

Bruno D and Randolph MF (1999) Dynamic and static load testing of model piles driven into dense sand. *Journal of Geotechnical and Geoenvironmental Engineering* **125(11)**: 988–998.

BSH (Federal Maritime and Hydrographic Agency) (2015) *Standard Design – Minimum Requirements Concerning the Constructive Design of Offshore Structures within the Exclusive Economic Zone (EEZ)*, Bsh-no. 7005. BSH, Hamburg and Rostock, Germany.

Clausen CJF, Aas PM and Karlsrud K (2005) Bearing capacity of driven piles in sand, the NGI approach. In *Proceedings of the International Symposium on Frontiers in Offshore Geotechnics (IS-FOG 2005)* (Cassidy M and Gourvenec S (eds)). CRC Press, Perth, Australia, pp. 677–681.

Deeks AD, White DJ and Bolton MD (2005) A comparison of jacked, driven and bored piles in sand. In *Proceedings of the 16th International Conference of Soil Mechanics and Geotechnical Engineering, Osaka, Japan*. IOS Press, Amsterdam, the Netherlands, pp. 2103–2106.

De Nicola A and Randolph MF (1994) Development of a miniature pile driving actuator. In *Proceedings of the International Conference on Centrifuge Modelling 1994* (Leung CF, Lee FH and Tan TS (eds)). CRC Press, Singapore, pp. 473–478.

de Nicola A and Randolph MF (1997) The plugging behaviour of driven and jacked piles in sand. *Géotechnique* **47(4)**: 841–856, https://doi.org/10.1680/geot.1997.47.4.841.

DIN (Deutsches Institut für Normung) (2014) Handbuch Eurocode 7-1 Entwurf, Berechnung und Bemessung in der Geotechnik – Teil 1: Allgemeine Regeln, Deutsche Fassung EN 1997-1:2005+AC:2009+A1:2013 (Eurocode 7: Geotechnical design-Part 1: General rules; German version EN 1997-1:2004+AC:2009+A1:2013). DIN, Berlin, Germany.

EA-Pfähle (2012) *Empfehlungen des arbeitskreises 'pfähle'– ea-pfähle der deutschen geschellschaft für geotechnik (dggt) (Recommendations on Piling from the Working Commission 'piles' of the German Geotechnical Society(dggt))*, 2nd edn. Ernst & Sohn, Hamburg, Germany (in German).

Finnie IMS and Randolph MF (1994) Punch-through and liquefaction induced failure of shallow foundations on calcareous sediments. *In Proceedings of the Seventh International Conference on the Behaviour of Offshore Structures, Cambridge, MA, USA* (Chryssostomidis C (ed.)). Massachusetts Institute of Technology, Cambridge, MA, USA, vol. 1, pp. 217–230.

Grabe J and Heins E (2016) Coupled deformation-seepage analysis of dynamic capacity tests on open-ended piles in saturated sand. *Acta Geotechnica* **12(1)**: 211–223.

Hartung M (1994) *Einflüsse der Herstellung auf die Pfahltragfähigkeit in Sand (Influences of the Installation Process on the Pile Bearing Capacity in Sand)*. PhD thesis, Mitteilung des Instituts für Grundbau und Bodenmechanik der Technischen Universität Braunschweig, Braunschweig, Germany (in German)

Heerema EP and de Jong A (1979) An advanced wave equation computer program which simulates dynamic pile plugging through a coupled mass-spring system. In *Proceedings of the International Conference on Numerical Methods in Offshore Piling, London, UK*, pp. 37–42.

Henke S and Grabe J (2013) Field measurements regarding the influence of the installation method on soil plugging in tubular piles. *Acta Geotechnica* **8(3)**: 335–352.

Jardine R, Chow F, Overy R and Standing J (2005) *ICP Design Methods for Driven Piles in Sands and Clays*. ICE Press, London, UK.

Kolymbas D (1991) Longitudinal impacts on piles. *Soil Dynamics and Earthquake Engineering* **10(5)**: 264–270.

Lee CJ, Chen HT, Lien HC, Wei YC and Hung WY (2014) Centrifuge modeling of the seismic responses of sand deposits with an intra-silt layer. *Soil Dynamics and Earthquake Engineering* **65**: 72–88.

Lehane BM and Gavin KG (2001) Base resistance of jacked pipe piles in sand. *Journal of Geotechnical and Geoenvironmental Engineering* **127(6)**: 473–480.

Paik K, Salgado R, Lee J and Kim B (2003) Behavior of open- and closed-eneded piles driven into sand. *Journal of Geotechnical and Geoenvironmental Engineering* **129(4)**: 296–306.

Paikowsky S and Chernauskaus LR (2008) Dynamic analysis of open ended pipe piles. In *Proceedings of the 8th International Conference on the Application of Stress Wave Theory to Piles in Lisbon, Portugal* (Santos JA (ed.)), IOS Press, Amsterdam, the Netherlands, pp. 59–76.

Paikowsky SG and Whitman RV (1990) The effects of plugging on pile performance and design. *Canadian Geotechnical Journal* **27(4)**: 429–440.

Pucker T, Bienen B and Henke S (2013) CPT based prediction of foundation penetration in siliceous sand. *Applied Ocean Research* **41**: 9–18.

Randolph MF (2003) Science and empiricism in pile foundation design. *Géotechnique* **53(10)**: 847–875, https://doi.org/10.1680/geot.2003.53.10.847.

Randolph MF and Deeks AJ (1992) Dynamic and static soil models for axial pile response. In *Application of Stress-Wave Theory to Piles* (Barends FBJ (ed.)). CRC Press, The Hague, the Netherlands, pp. 3–14.

Rausche F, Likins G, Liang L and Hussein M (2010) Static and dynamic models for capwap signal matching. In *Art of Foundation Engineering Practice* (Hussein MH, Anderson JB and Camp WM (eds)). ASCE, Reston, VA, USA, pp. 534–553.

Schneider JA, Lehane BM and XU X (2005) The UWA-05 method for prediction of axial capacity of driven piles in sand. In *Proceedings of the International Symposium on Frontiers in Offshore Geotechnics (IS-FOG 2005)* (Cassidy M and Gourvenec S (eds)). CRC Press, Perth, Australia, pp. 683–688.

Sharp MK, Dobry R and Abdoun T (2003) Liquefaction centrifuge modeling of sands of different permeability. *Journal of Geotechnical and Geoenvironmental Engineering* **139(8)**: 1215–1234.

Stahlmann J, Kirsch F, Schallert M, Klingmüller O and Elmer KH (2004) Pfahltests – modern dynamisch und/oder konservativ statisch (Pile tests – modern dynamic and/or conservative static). In *Tagungsband zum 4. Kolloquium 'Bauen in Boden und Fels' der Technischen Akademie Esslingen, Ostfildern, Germany* (Schad H (ed.)), pp. 23–40.